nature medicine

ARTICLES

Salt-sensitive hypertension is triggered by Ca^{2+} entry via Na^+/Ca^{2+} exchanger type-1 in vascular smooth muscle

Takahiro Iwamoto[1,3], Satomi Kita[1,5], Jin Zhang[2], Mordecai P Blaustein[2], Yuji Arai[4], Shigeru Yoshida[5], Koji Wakimoto[6], Issei Komuro[7] & Takeshi Katsuragi[1]

Excessive salt intake is a major risk factor for hypertension. Here we identify the role of Na^+/Ca^{2+} exchanger type 1 (NCX1) in salt-sensitive hypertension using SEA0400, a specific inhibitor of Ca^{2+} entry through NCX1, and genetically engineered mice. SEA0400 lowers arterial blood pressure in salt-dependent hypertensive rat models, but not in other types of hypertensive rats or in normotensive rats. Infusion of SEA0400 into the femoral artery in salt-dependent hypertensive rats increases arterial blood flow, indicating peripheral vasodilation. SEA0400 reverses ouabain-induced cytosolic Ca^{2+} elevation and vasoconstriction in arteries. Furthermore, heterozygous NCX1-deficient mice have low salt sensitivity, whereas transgenic mice that specifically express NCX1.3 in smooth muscle are hypersensitive to salt. SEA0400 lowers the blood pressure in salt-dependent hypertensive mice expressing NCX1.3, but not in SEA0400-insensitive NCX1.3 mutants. These findings indicate that salt-sensitive hypertension is triggered by Ca^{2+} entry through NCX1 in arterial smooth muscle and suggest that NCX1 inhibitors might be useful therapeutically.

Hypertension is the most common chronic disease, and is the leading risk factor for death that is due to stroke, myocardial infarction or end-stage renal failure[1,2]. The critical importance of excess salt intake in the pathogenesis of hypertension is widely recognized[3–6], but the mechanism by which excess salt intake elevates blood pressure has puzzled researchers. Recently discovered cardiotonic steroids (CTS), such as endogenous ouabain[7], and other steroids[8–10], including marinobufagenin, proscillaridin A and bufalin, have been proposed as candidate intermediaries. In humans, a chronic high-salt diet causes a rise in plasma CTS[11–13]. Moreover, ~50% of patients with essential hypertension have substantially elevated levels of endogenous ouabain[14,15]. Plasma CTS are also high in several salt-dependent hypertensive animals[7,13,16]. Indeed, PST2238, a ouabain antagonist, lowers blood pressure in salt-dependent hypertensive rats and in certain patients with essential hypertension[17,18]. Generally, it is believed that CTS inhibit the plasma membrane Na^+/K^+ ATPase, the 'sodium-potassium pump,' and lead to an increase in cytosolic Na^+ concentration ($[Na^+]_{cyt}$). Cellular Na^+ accumulation raises the cytosolic Ca^{2+} concentration ($[Ca^{2+}]_{cyt}$) through the involvement of the Na^+/Ca^{2+} exchanger (NCX), and thereby increases contraction in vascular or heart muscle. This may lead to hypertension[19], but the hypothesis has not yet been critically tested because little is understood of the function of NCX in these processes.

NCX is a plasma membrane transporter expressed in various cell types. Membrane potential and transmembrane gradients of Na^+ and Ca^{2+} control this bidirectional exchanger. The mammalian NCX family comprises three isoforms[20]. NCX1 is abundant in the heart, but is also expressed in many other tissues. In contrast, expression of NCX2 and NCX3 is restricted to brain and skeletal muscle. Extensive alternative splicing of NCX1 generates tissue-specific variants[21–23]; the heart expresses exclusively NCX1.1, and vascular tissue predominantly NCX1.3 and NCX1.7. Although the importance of this diversity is unclear, it may reflect different requirements for the maintenance of Ca^{2+} homeostasis in various cell types[20]. In cardiomyocytes, NCX1 has the primary role in Ca^{2+} extrusion during excitation-contraction coupling[24]. Under pathological conditions such as cardiac ischemia-reperfusion injury[25,26], NCX1 is thought to cause Ca^{2+} overload resulting from elevated $[Na^+]_{cyt}$; this leads to cardiac dysfunction. In other tissues, including vascular smooth muscle (VSM), NCX1 is also believed to extrude Ca^{2+} from the cytosol[25], but the physiological roles of vascular NCX1 are still unclear.

Recently, SEA0400, a specific NCX inhibitor that preferentially blocks the Ca^{2+} entry mode[27,28], was developed. We now report that SEA0400 lowers arterial blood pressure in salt- or ouabain-dependent hypertensive models, but not in normotensive rats or in other types of hypertensive rats. SEA0400 reverses the cytosolic Ca^{2+} elevation and vasoconstriction induced by nanomolar ouabain. Furthermore, we found that heterozygous mice with reduced expression of NCX1 resist development of salt-dependent hypertension. Conversely, transgenic mice with VSM-specific expression of NCX1 readily develop hypertension after high salt intake. These data provide compelling

[1]Department of Pharmacology, School of Medicine, Fukuoka University, Fukuoka 814-0180, Japan. [2]Department of Physiology, University of Maryland School of Medicine, Baltimore, Maryland 21201, USA. Departments of [3]Molecular Physiology and [4]Bioscience, National Cardiovascular Center Research Institute, Osaka 565-8565, Japan. [5]Medicinal Research Laboratories, Taisho Pharmaceutical Co., Ltd., Saitama 330-8530, Japan. [6]Discovery Research Laboratory, Tanabe Seiyaku Co., Ltd., Osaka 532-8505, Japan. [7]Department of Cardiovascular Science and Medicine, Chiba University Graduate School of Medicine, Chiba 260-8670, Japan. Correspondence should be addressed to T.I. (tiwamoto@cis.fukuoka-u.ac.jp).

Published online 10 October 2004; doi:10.1038/nm1118

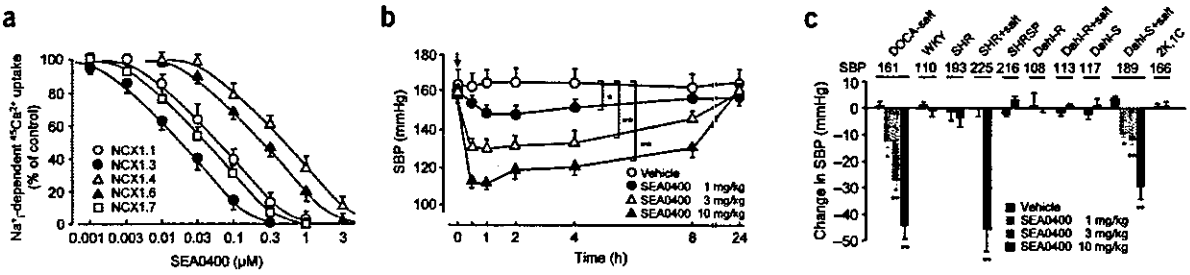

Figure 1 NCX1 inhibition and antihypertensive effects of SEA0400. (**a**) Concentration-response curves of SEA0400 for intracellular Na^+ (Na^+_i)-dependent $^{45}Ca^{2+}$ uptake into fibroblasts overexpressing variously spliced isoforms of human NCX1. Expression levels and NCX activities in these transfectants are shown in **Supplementary Figure 1** online. (**b**) Recordings over 24 h (9 a.m. to 9 a.m.) of SBP after oral administration of vehicle or SEA0400 (1–10 mg/kg) in DOCA-salt hypertensive rats. (**c**) Peak changes in SBP in various types of hypertensive rats treated with oral SEA0400. SHR, Dahl salt-resistant rats (Dahl-R) and Dahl salt-sensitive rats (Dahl-S) were fed a normal (0.3% NaCl) or high-salt diet (8% NaCl; +salt) for 4–6 weeks. Change in SBP in mmHg for the respective rats is indicated. Bars represent means ± s.e.m. (n = 4–6). WKY, Wistar Kyoto rats; SHRSP, stroke-prone SHR; 2K,1C, two-kidney, one-clip rats. $^*P < 0.05$, $^{**}P < 0.01$ compared with each vehicle group.

evidence that salt-dependent hypertension is triggered by Ca^{2+} entry through NCX1 in VSM cells. This finding also suggests that vascular NCX1 is a new therapeutic or diagnostic target for salt-sensitive hypertension.

RESULTS

Antihypertensive effects of SEA0400

In VSM cells, NCX1.3 and NCX1.7 are the dominant splicing isoforms[21–23]. By measuring intracellular Na^+-dependent Ca^{2+} uptake into fibroblasts overexpressing splicing isoforms of NCX1, we found that SEA0400, a specific inhibitor for Ca^{2+} entry through NCX1, preferentially blocks the vascular isoforms, especially NCX1.3 (**Fig. 1a** and **Supplementary Fig. 1** online). This finding indicates that SEA0400 is an excellent pharmacological tool for studying the vascular function of NCX1.

To evaluate the role of NCX1 in hypertension, we tested the effects of SEA0400 on various hypertensive models. A single oral dose of SEA0400 (1–10 mg/kg) caused a dose-dependent and long-lasting decrease in systolic blood pressure (SBP) in deoxycorticosterone acetate (DOCA)-salt hypertensive rats (**Fig. 1b**). Intravenous administration of SEA0400 (0.3–3 mg/kg) also lowered SBP in anesthetized DOCA-salt hypertensive rats (data not shown). Notably, however, SEA0400 did not significantly affect SBP in spontaneously hypertensive rats (SHR) or Wistar Kyoto rats ($P > 0.05$; **Fig. 1c**). We also examined the antihypertensive effect of SEA0400 in other hypertensive models. SEA0400 significantly decreased SBP in Dahl salt-sensitive rats and SHR when they were chronically loaded with high salt ($P < 0.01$; **Fig. 1c**). On the other hand, SEA0400 had no effect on SBP in stroke-prone SHR, salt-loaded or salt-unloaded Dahl salt-resistant rats, salt-unloaded Dahl salt-sensitive rats, or two-kidney, one-clip renal hypertensive rats. Thus, SEA0400 selectively suppresses salt-dependent hypertension.

The effect of chronic treatment with SEA0400 was also tested in DOCA-salt hypertensive rats. Administration of SEA0400 (3 or 10 mg/kg) for 3 weeks efficiently overcame the development of hypertension, vascular hypertrophy and renal dysfunction induced by DOCA-salt treatment (**Supplementary Fig. 2** and **Supplementary Tables 1 and 2** online). This suggests that SEA0400 has therapeutic potential as a new antihypertensive drug.

Direct vasodilation by SEA0400

To analyze its antihypertensive mechanism, we infused SEA0400 into the femoral artery of anesthetized DOCA-salt hypertensive rats (**Fig. 2a**). Intrafemoral infusion of SEA0400 (10 μg/kg/min) markedly increased femoral blood flow (FBF), indicating that SEA0400 caused peripheral vasodilation. A similar infusion did not affect FBF in normotensive sham rats. On the other hand, when the femoral artery of the sham rat (recipient) was crossperfused with aortic blood from the DOCA-salt hypertensive rat (donor), the intrafemoral infusion of SEA0400 significantly increased the FBF ($P < 0.05$; **Fig. 2b**). SEA0400 had no effect in the crossperfusion between two sham rats. This suggests that humoral vasoconstrictors participate in DOCA-salt hypertension; these vasoconstrictor effects can be antagonized by SEA0400.

Endogenous CTS are thought to contribute to the pathogenesis of salt-sensitive hypertension in patients and experimental animals[7,11–16]. Indeed, chronic administration of ouabain to rats causes hypertension[29,30]. Therefore, we examined the effect of SEA0400 on ouabain-induced hypertension. SEA0400 (1 or 10 mg/kg) suppressed hypertension in a dose-dependent manner in Sprague-Dawley rats on long-term ouabain treatment (**Fig. 3a**). SEA0400 did not affect the vasopressor responses to intravenous administration of norepinephrine, angiotensin II and endothelin-1 in anesthetized Sprague-Dawley rats (data not shown). Furthermore, to check the antagonistic interaction between ouabain and SEA0400, either ouabain or SEA0400, or both, were infused into the femoral arteries of anesthetized beagles. Intrafemoral infusion of SEA0400 (50 μg/kg/min) alone did not affect FBF. Infusion of either ouabain (0.5 μg/kg/min), however, reduced the FBF by approximately 50%; addition of SEA0400 then restored FBF to the basal level (**Fig. 3b**).

Effects of SEA0400 on pressurized small arteries

In VSM cells, inhibition of sarcolemmal Na^+/K^+ ATPases by endogenous CTS would be expected to increase $[Na^+]_{cyt}$ and subsequently to raise $[Ca^{2+}]_{cyt}$ through the NCX. To test this hypothesis, we examined the effects of low-dose ouabain and SEA0400 on $[Ca^{2+}]_{cyt}$ (measured as fluo-4 fluorescence) and vasoconstriction in intact, pressurized mouse small mesenteric arteries with myogenic tone. Ouabain (100 nM) increased fluo-4 fluorescence by ~12% and myogenic tone by 20–25% (**Fig. 4**). The physiological consequences of even small changes are profound because of Poiseuille's law[31]: resistance to blood flow, R, is inversely proportional to the fourth power of the internal radius, r ($R \propto 1/r^4$). Thus, a 5–10% rise in $[Ca^{2+}]_{cyt}$ should augment myogenic tone[32] enough to increase R (and blood pressure)[31] by ~20–50% (**Fig. 4**).

SEA0400 (300 nM) abolished the effects induced by low-dose ouabain. A video clip of the fluo-4 fluorescence data shown in

Figure 2 Vascular responses to intrafemoral infusion of SEA0400 in anesthetized DOCA-salt hypertensive or uninephrectomized sham rats. (a) SEA0400 or vehicle was infused at a rate of 20 µl/min into the femoral artery while monitoring the heart rate (HR), mean blood pressure (MBP), and femoral blood flow (FBF). (b) SEA0400 was infused into the femoral artery of the recipient (sham rat) crossperfused with the blood from the donor (DOCA-salt hypertensive rat or sham rat). Bars represent means ± s.e.m. ($n = 4$). $^*P < 0.05$; $^{**}P < 0.01$ compared with pretreatment values.

Figure 4b is available online as **Supplementary Movie 1**. In control arteries, SEA0400 also lowered $[Ca^{2+}]_{cyt}$ slightly (data not shown) and reduced normal myogenic tone by about 10% (Fig. 4c). SEA0400 had no effect on 75 mM K^+-induced vasoconstriction (data not shown), consistent with previous reports on SEA0400 selectivity[27,33]. These results suggest that the increased myogenic tone induced by low-dose ouabain, and even a part of the normal resting tone, may depend upon Ca^{2+} entry mediated by NCX.

Prevention of DOCA-salt hypertension in NCX1 heterozygous mice

To study the functional significance of NCX1 in salt-sensitive hypertension, the hypertensive responsiveness to DOCA-salt treatment was examined in heterozygous NCX1-deficient (*Slc8a1*$^{+/-}$) mice. The NCX1 protein level in the aorta, as well as in other organs[34], of *Slc8a1*$^{+/-}$ mice was about 50% of that seen in wild-type mice (Fig. 5). On the other hand, there were no differences in expression levels of Na^+/K^+-ATPase (α_2 and α_3), L-type Ca^{2+} channel (α_{1C}) and sarcolemmal Ca^{2+}-ATPase in aortas from *Slc8a1*$^{+/-}$ mice (data not shown). Basal SBP of *Slc8a1*$^{+/-}$ mice was no different from that of wild-type mice. DOCA-salt treatment produced a progressive elevation in SBP in wild-type mice ($P < 0.01$), whereas the same treatment did not significantly alter the SBP of *Slc8a1*$^{+/-}$ mice ($P > 0.05$; Fig. 5a). When the sodium level in drinking water for DOCA-salt treatment was increased from 1% to 2%, *Slc8a1*$^{+/-}$ mice responded with a mild increase in SBP (108 ± 3 mmHg ($n = 5$) at 3 weeks, $P < 0.05$), though wild-type mice experienced severe hypertension (128 ± 5 mmHg ($n = 5$), $P < 0.01$). In contrast, hypertensive responses to chronic angiotensin II infusion were similar in *Slc8a1*$^{+/-}$ and wild-type mice (Fig. 5b).

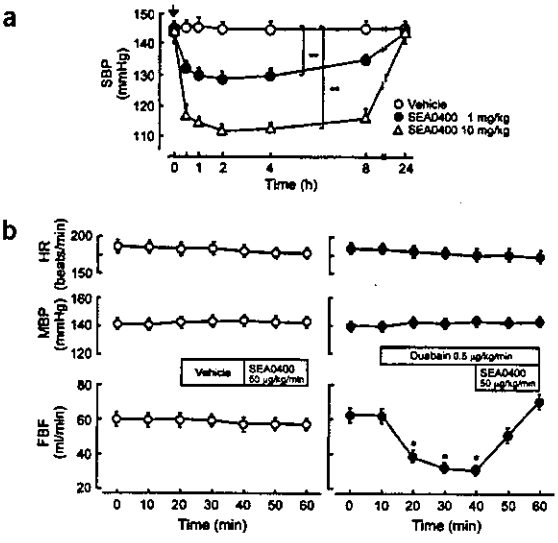

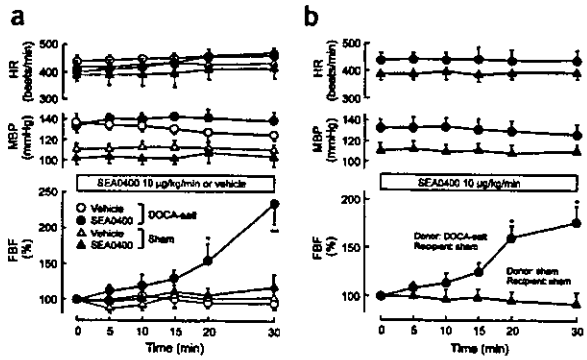

Salt hypersensitivity in VSM-specific NCX1.3 transgenic mice

To test further whether vascular NCX1 has a critical role in salt-sensitive hypertension, we created transgenic mice (*N1.3*$^{Tg/Tg}$) expressing canine *Ncx1.3* driven by the smooth muscle α-actin promoter (Fig. 6a). Southern blotting indicated that four founders had 2–4 copies of the transgene (data not shown). From among them, two independent transgenic lines were selected for detailed study. Western blot analysis showed that NCX1.3 protein was overexpressed in the aortas, but not in the hearts, of these transgenic mice at 6- to 8-fold the level of endogenous NCX1 (**Supplementary Fig. 3** online). Immunohistochemical staining indicated dense localization of NCX1.3 in the medial layer of aortas from *N1.3*$^{Tg/Tg}$ mice (Fig. 6b). On the other hand, no difference was observed in protein levels of Na^+/K^+-ATPase (α_2 and α_3), L-type Ca^{2+} channel (α_{1C}) and sarcolemmal Ca^{2+} ATPase in aortas from *N1.3*$^{Tg/Tg}$ mice by western blotting (data not shown). Functional augmentation was correlated with increased NCX1 protein levels in aortas from *N1.3*$^{Tg/Tg}$ mice, as shown by measuring the rate and degree of contraction evoked by Na^+ removal in aortic rings pretreated with ouabain (**Supplementary Fig. 3** online). Furthermore, the 10 µM ouabain-induced $[Ca^{2+}]_{cyt}$ rise in mesenteric arteries from *N1.3*$^{Tg/Tg}$ mice was notably greater than in those from wild-type mice (Fig. 6c,d).

Notably, the basal SBP of *N1.3*$^{Tg/Tg}$ mice (103 ± 1.4 mmHg, $n = 6$) was slightly, but significantly ($P < 0.05$), higher than that of wild-type mice (92 ± 1.1 mmHg, $n = 5$). When these mice were fed an 8% NaCl diet with 1% NaCl drinking water, SBP in *N1.3*$^{Tg/Tg}$ mice, but not in wild-type mice, progressively rose to 124 ± 3.5 mmHg ($n = 6$) at 4 weeks after the start of salt loading (Fig. 6e). Oral administration of SEA0400 (10 mg/kg) markedly lowered the SBP of salt-loaded *N1.3*$^{Tg/Tg}$ mice, but not of salt-loaded wild-type mice (Fig. 6f). Intravenous administration of SEA0400 (0.3 mg/kg) also lowered SBP in anesthetized *N1.3*$^{Tg/Tg}$ mice by about 20 mmHg (data not shown). In addition, oral administration of SEA0400 suppressed basal SBP (mild hypertension) of *N1.3*$^{Tg/Tg}$ mice, but not of wild-type mice, and abolished the difference between the two groups (**Supplementary Fig. 3** online).

Figure 3 Effects of SEA0400 on ouabain-induced hypertension and vasoconstriction. (a) Recordings over 24 h of SBP after oral administration of SEA0400 in hypertensive rats infused subcutaneously with ouabain (30 µg/kg/d for 5 weeks). $^{**}P < 0.01$ compared with the vehicle group ($n = 5$). (b) Femoral blood flow (FBF) response to intrafemoral infusion of SEA0400 or vehicle at a rate of 0.2 ml/kg/min in the presence (right) or absence (left) of ouabain in anesthetized beagles. MBP and HR were monitored during the experimental periods. $^*P < 0.05$ compared with pretreatment values ($n = 4$).

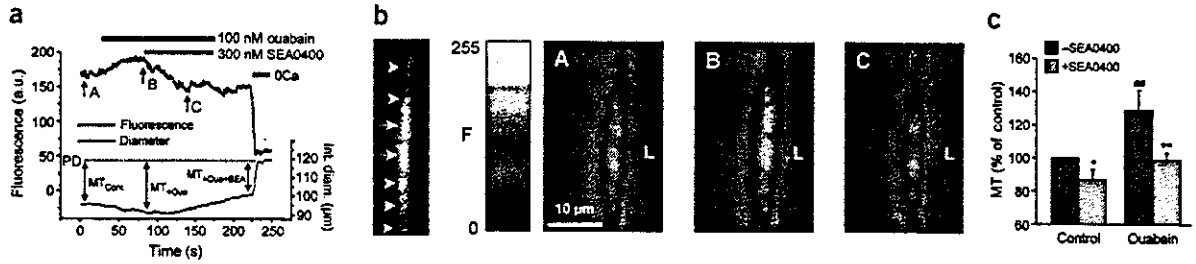

Figure 4 Effects of low-dose ouabain and SEA0400 on cytosolic Ca^{2+} level and myogenic tone (MT) in pressurized mouse small mesenteric arteries. (**a**) Simultaneous recording of fluorescence and internal diameter (Int. diam.) changes in a fluo-4 loaded artery (pressurized to 70 mmHg) by laser confocal microscopy. The fluo-4 fluorescence, indicated in arbitrary units (a.u.), reflects $[Ca^{2+}]_{cyt}$. Periods of exposure to ouabain, SEA0400 and Ca^{2+}-free medium (0Ca) are indicated by colored bars. The dotted line shows the passive internal diameter (PD) in 0Ca. (**b**) Fluorescent image on the left shows individual myocytes loaded with fluo-4 (arrows); the artery has only a single layer of myocytes. Pseudocolor images (**A–C**) indicate the relative $[Ca^{2+}]_{cyt}$ at the times shown in **a**. L, artery lumen. A video clip of the original data from this experiment is available at **Supplementary Movie 1** online. (**c**) Summary of the effects of ouabain and SEA0400 on MT, normalized to MT under control conditions. Mean PD was 107 ± 4 μm. At 70 mmHg, arteries constricted to 77 ± 4 μm internal diameter (≈ control MT). Ouabain caused a further constriction to 70 ± 4 μm; based on Poiseuille's law[31], this should increase resistance to blood flow (and blood pressure) by ~46%. $^{*}P < 0.05$; $^{**}P < 0.01$ versus pretreatment values ('–SEA0400'). $^{\#\#}P < 0.01$ versus control values ($n = 6$).

To verify that the antihypertensive effect of SEA0400 results from the inhibition of genetically overexpressed NCX1.3, we generated transgenic mice (*mN1.3*$^{Tg/Tg}$) expressing an SEA0400-insensitive G833C mutant[28] (Fig. 6a). Three independent lines of *mN1.3*$^{Tg/Tg}$ mice were selected for detailed analysis. The phenotypes of *mN1.3*$^{Tg/Tg}$ mice were very similar to those of *N1.3*$^{Tg/Tg}$ mice, except for their vascular response to SEA0400 (Fig. 6b–e and Supplementary Fig. 3 online); this drug blocked the contraction evoked by Na^+ removal in ouabain-pretreated aortic rings and the ouabain-induced $[Ca^{2+}]_{cyt}$ rise in arterial strips from *N1.3*$^{Tg/Tg}$ mice, but not from *mN1.3*$^{Tg/Tg}$ mice. In *mN1.3*$^{Tg/Tg}$ mice, SEA0400 (10 mg/kg) did not show a reduction in high salt–induced hypertension (Fig. 6f) and basal SBP (Supplementary Fig. 3 online). This shows that SEA0400 acts on the overexpressed NCX1.3 in VSM cells.

Given the possibility of nonspecific effects associated with NCX1 overexpression, as a further control we generated transgenic mice (*N1.1*$^{Tg/Tg}$) expressing canine *Ncx1.1* driven by the α-myosin heavy-chain promoter. In established *N1.1*$^{Tg/Tg}$ lines, hearts, but not aortas, showed a 2- to 3-fold increase in the level of NCX1 protein. Basal SBP of *N1.1*$^{Tg/Tg}$ mice was normal, and was similar to that of wild-type mice. Furthermore, the blood pressure of *N1.1*$^{Tg/Tg}$ mice, like that of wild-type mice, was resistant to long-term salt-loading and insensitive to the effect of SEA0400 (Supplementary Fig. 4 online).

DISCUSSION

The critical importance of sodium retention, resulting from excess salt intake or reduced renal salt excretion, in the pathogenesis of hypertension is widely recognized[3–6]. But the molecular mechanisms underlying salt-sensitive hypertension remain obscure. Here we show that SEA0400 lowers arterial blood pressure in various models of salt-dependent hypertension. SEA0400 does not, however, affect arterial blood pressure in normotensive rats or in other types of hypertensive rats. Furthermore, NCX1 heterozygous mice are resistant to DOCA-salt hypertension, but not to angiotensin II–induced hypertension. These findings suggest that vascular NCX1 is critical in the development of salt-sensitive hypertension.

The contraction of VSM cells is initiated by a rise in $[Ca^{2+}]_{cyt}$ through voltage-gated or receptor-operated Ca^{2+} channels in the sarcolemma, or both, or through Ca^{2+}-release channels in the sarcoplasmic reticulum membrane[35,36]. In general, sarcolemmal NCX, like the sarcolemmal or sarcoplasmic reticulum Ca^{2+}ATPases, is thought to contribute to Ca^{2+} extrusion from the cytosol in the relaxation process. Data obtained using antisense oligonucleotides indicate that NCX1 knockdown prolongs agonist responses by delaying the return of $[Ca^{2+}]_{cyt}$ to the resting level in cultured VSM cells[37,38].

To confirm the *in vivo* function of vascular NCX1 in mice, we generated VSM-specific transgenic mice expressing either wild-type NCX1.3 (*N1.3*$^{Tg/Tg}$) or the SEA0400-insensitive G833C mutant (*mN1.3*$^{Tg/Tg}$). Comparative experiments using these mutants and SEA0400 are useful for assessing the pharmacological significance of NCX inhibition[28]. Interestingly, both kinds of transgenic mice were mildly hypertensive (by about 10 mmHg) compared with wild-type mice. They also exhibited high salt–induced hypertension as a result of increased salt sensitivity. Administration of SEA0400 normalized

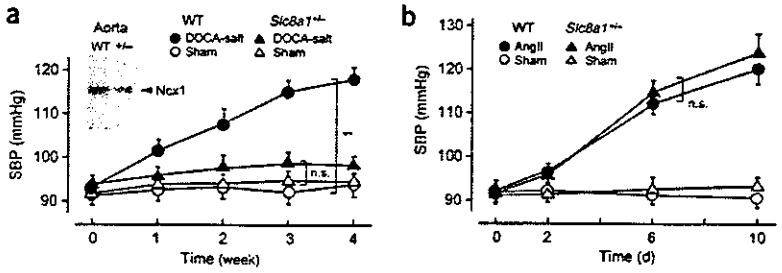

Figure 5 Prevention of DOCA-salt hypertension in *Slc8a1*$^{+/-}$ mice. (**a**) Uninephrectomized *Slc8a1*$^{+/-}$ and wild-type (WT) mice received DOCA (75 mg/kg) subcutaneously twice a week, and were given tap water containing 1% NaCl for 4 weeks. Sham mice were uninephrectomized but not given DOCA and salt. (**b**) Miniosmotic pumps containing angiotensin II (AngII) or vehicle (sham) were subcutaneously implanted in *Slc8a1*$^{+/-}$ and WT mice on day 0. Systolic blood pressure (SBP) was monitored by tail cuff. $^{**}P < 0.01$ versus control groups ($n = 5$ or 6).

blood pressure and suppressed salt-dependent hypertension in $N1.3^{Tg/Tg}$ mice, but not in $mN1.3^{Tg/Tg}$ mice. The latter mutation interferes with SEA0400 binding but does not affect Na^+/Ca^{2+} exchange[28]. In contrast, heart-specific transgenic mice expressing NCX1.1 were salt-insensitive, and their blood pressure did not respond to SEA0400. These results indicate that vascular NCX1 acts primarily as a Ca^{2+} entry pathway for regulating arterial tone, especially under sodium-retaining conditions. SEA0400 exerts its antihypertensive effect by blocking this Ca^{2+} entry in arterial myocytes.

Indeed, SEA0400 reverses the vasoconstriction and hypertension induced by exogenous ouabain, which may facilitate Ca^{2+} entry through NCX due to elevated $[Na^+]_{cyt}$, although SEA0400 does not directly affect the activity of Na^+/K^+-ATPases[27]. Notably, in VSM cells the NCX1 is colocalized with Na^+/K^+-ATPase α_2 and α_3 isoforms, which have high affinity for ouabain[39], in plasma membrane microdomains adjacent to the sarcoplasmic reticulum[40,41]. Functional coupling between NCX and Na^+/K^+-ATPase has been reported in vascular and cardiac myocytes[37,42–44]. As described above, endogenous plasma CTS are increased under pathological conditions such as salt-sensitive hypertension[7,11–16]. When CTS inhibit Na^+/K^+-ATPases (α_2 and α_3) in VSM cells, the elevation of local Na^+ in the submembrane area is expected to facilitate Ca^{2+} entry through NCX1, resulting in vasoconstriction. Our data indicate that blood from DOCA-salt hypertensive rats contains humoral vasoconstrictors whose action is counteracted by SEA0400. Also, using isolated, pressurized mouse small mesenteric arteries, we confirmed that 100 nM ouabain increases both $[Ca^{2+}]_{cyt}$ and myogenic tone by about 20–25% and that SEA0400 completely abolishes these effects. In addition, the 10 μM ouabain–induced $[Ca^{2+}]_{cyt}$ rise in arterial strips from transgenic mice was greater than in those from wild-type mice. SEA0400 blocked these $[Ca^{2+}]_{cyt}$ rises in $N1.3^{Tg/Tg}$ and wild-type mice, but not in $mN1.3^{Tg/Tg}$ mice. These data provide evidence that ouabain triggers Ca^{2+} entry through NCX1 in VSM cells by inhibiting high ouabain–affinity Na^+ pumps (α_2 or α_3) and elevating submembrane Na^+. Although ouabain has also been reported to mediate other signaling pathways[45], they apparently are not involved in the VSM mechanism described here.

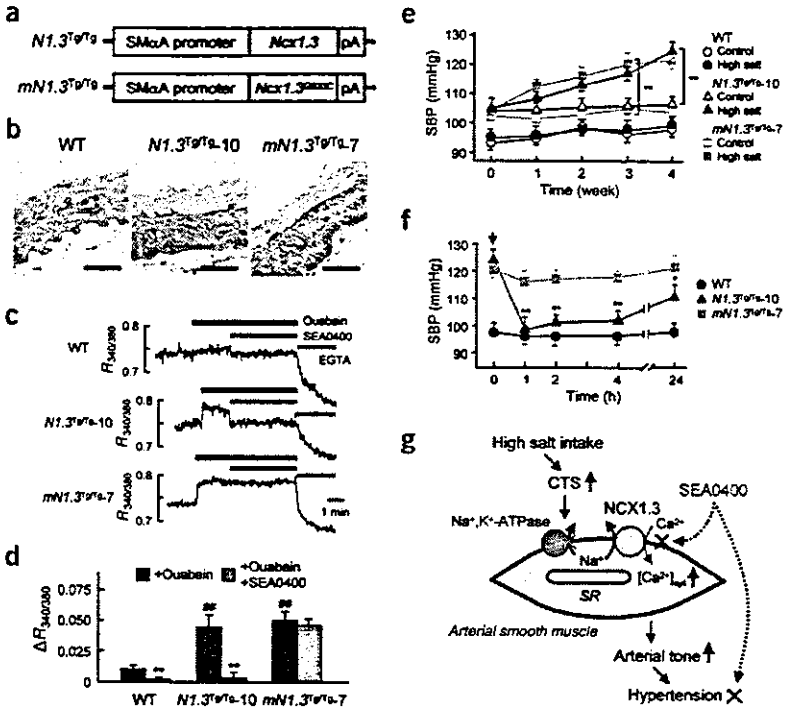

Figure 6 Enhanced salt-sensitivity in $N1.3^{Tg/Tg}$ or $mN1.3^{Tg/Tg}$ mice. (a) Schematic representation of the transgene used to generate VSM-specific transgenic mice. The *Ncx1.3* or its G833C mutant ($Ncx1.3^{G833C}$) was brought under the control of human smooth muscle α-actin (SMαA) promoter. (b) Immunohistochemical localization of NCX1 proteins in the medial layer of thoracic aortas from wild-type (WT) mice and two representative transgenic lines ($N1.3^{Tg/Tg}$-10 and $mN1.3^{Tg/Tg}$-7). Scale bars, 50 μm. (c) Effects of ouabain and SEA0400 on $[Ca^{2+}]_{cyt}$ (fura-PE3 fluorescence ratio ($R_{340/380}$)) in isolated mesenteric arteries from transgenic and WT mice. Periods of exposure to 10 μM ouabain, 1 μM SEA0400 and 4 mM EGTA are indicated by bars. All experiments were performed in the presence of 10 μM nicardipine to suppress L-type Ca^{2+} channels. (d) Summary of the experiments shown in (c). $^{**}P < 0.01$ versus pretreatment values ('+Ouabain'). $^{\#\#}P < 0.01$ versus WT groups ($n = 5$). (e,f) Salt-induced hypertension and antihypertensive effects of SEA0400 (10 mg/kg) in transgenic and WT mice treated with a high-salt diet (8% NaCl) and tap water containing 1% NaCl for 4 weeks. $^*P < 0.05$; $^{**}P < 0.01$ ($n = 5$ or 6). (g) Proposed pathway responsible for salt-sensitive hypertension. High salt intake causes the levels of endogenous CTS to rise in the plasma. This results in the increase in subplasma membrane $[Na^+]$ of arterial smooth muscle. The restricted $[Na^+]$ accumulation elevates $[Ca^{2+}]_{cyt}$ by vascular NCX1 isoform–mediated Ca^{2+} entry. This enhances arterial tone and causes hypertension. SEA0400 blocks this Ca^{2+} entry and exerts an antihypertensive effect in salt-sensitive hypertension.

SEA0400 does not affect arterial blood pressure in normotensive or salt-independent hypertensive animals. Intrafemoral infusion of SEA0400 in normal rats and beagles does not change arterial blood flow unless the arteries are perfused with exogenous ouabain or aortic blood from salt-dependent hypertensive animals. In addition, NCX1 heterozygous mice maintain normal blood pressure. Thus, the Ca^{2+} entry mode of NCX1 in VSM cells apparently has little role in blood pressure control in normotensive or in salt-insensitive hypertensive animals, probably owing to low plasma levels of CTS and to the overriding effects of reflex regulatory mechanisms. Nevertheless, the Ca^{2+} entry mode of NCX1 could have a role in regional blood flow even in normotensive and salt-insensitive animals, because SEA0400 slightly suppresses basal myogenic tone with a small reduction of $[Ca^{2+}]_{cyt}$ in pressurized mouse small mesenteric arteries.

In conclusion, our results show that the Ca^{2+} entry mode of vascular NCX1 is involved in the contractile regulation of small arteries and in the development of salt-dependent hypertension. Notably, recent human genome-wide linkage analysis of genes that affect blood pressure identified four regions, one of which includes *SLC8A1*, as loci containing candidate genes that influence blood pressure[46]. In humans and animals, endogenous CTS levels increase in plasma during salt retention[7,11–16]. Inhibition of Na^+ pumps by CTS should elevate local Na^+ and, through NCX1, $[Ca^{2+}]_{cyt}$ in VSM cells, thereby

promoting vasoconstriction (Fig. 6g). In this pathway, vascular NCX1 is a key mediator. SEA0400 selectively blocks NCX1.3, the vascular isoform of NCX1, and suppresses salt-dependent hypertension and associated secondary organ damage. Thus, the Ca^{2+} entry mode of vascular NCX1 may be a useful target for the development of therapies for salt-sensitive hypertension. Indeed, response to inhibitors of NCX1 may be diagnostic for salt-sensitive hypertension and involvement of the pathway illustrated in Figure 6g.

METHODS

$^{45}Ca^{2+}$ uptake. To examine the splice isoform selectivity of SEA0400, we cloned *NCX1.1*, *NCX1.3*, *NCX1.4*, *NCX1.6* and *NCX1.7* into pcDNA3.1 (Invitrogen) by PCR using human aortic cDNAs (Clontech). We transfected these plasmids with Lipofectin (Invitrogen) into CCL39 fibroblasts and we selected cells stably expressing NCX1 using a Ca^{2+}-killing procedure[47]. Intracellular Na^+-dependent $^{45}Ca^{2+}$ uptake into cells was assayed as described[47] (see Supplementary Methods online).

Experimental hypertensive models. To produce DOCA-salt hypertensive animals, 5-week-old male Sprague-Dawley rats or 12-week-old male mice were unilaterally nephrectomized under anesthesia with sodium pentobarbital. After allowing the animals a 1-week recovery, we administered DOCA (15 mg/kg for rats or 75 mg/kg for mice) with corn oil subcutaneously twice a week for 4 weeks. These animals then drank tap water containing 1% NaCl. Control animals (sham) were uninephrectomized but not given DOCA and salt. In the preparation of two-kidney, one-clip renal hypertensive rats, we anesthetized male Sprague-Dawley rats with sodium pentobarbital, and partially occluded the left renal artery by a silver clip (0.2 mm in diameter) for 4 weeks. To produce ouabain-induced hypertension, we infused ouabain subcutaneously at a rate of 30 μg/kg/day into male Sprague-Dawley rats by miniosmotic pumps (ALZET 2002) for 5 weeks. Ouabain was dissolved in sterile phosphate-buffered saline. To produce angiotensin II–induced hypertension, we subcutaneously implanted miniosmotic pumps containing either vehicle (0.01 N acetic acid in saline solution) or angiotensin II (750 μg/kg/d for 10 d) in male mice. We measured SBP at room temperature by a tail cuff method using an MK2000 blood pressure monitor (Muromachi Kikai). Rats or mice were acclimated to the procedures of blood pressure measurement for a week preceding actual data collection. We administered SEA0400 orally or intravenously with 5% gum arabic or a lipid emulsion containing 20% soybean oil (vehicle), respectively.

Intrafemoral infusion. To determine the peripheral vasodilation, we infused SEA0400 (10 μg/kg/min) or vehicle at a rate of 20 μl/min through a polyethylene tube in the right femoral artery of DOCA-salt hypertensive rats or uninephrectomized sham rats, anesthetized with sodium pentobarbital. In other experiments, we infused SEA0400 into the right femoral artery of the sham rat (recipient), which was crossperfused with vena caval and aortic blood of the donor rat and stabilized for 30 min. In yet other experiments, we infused SEA0400 (50 μg/kg/min) alone or in combination with ouabain (0.5 μg/kg/min) at a rate of 0.2 ml/min into the left femoral artery of anesthetized male beagles (9–10 kg). In all these experiments, FBF, systemic blood pressure and heart rate were monitored directly with a square-wave flowmeter and a pressure transducer (Nihon Koden), respectively.

Transgenic mice. We constructed the transgene by inserting canine *Ncx1.3* or its G833C mutant[28] between the human smooth muscle α-actin promoter and the SV40 polyadenylation sequence of the plasmid (T. Miwa). We also prepared an additional transgene by inserting canine *Ncx1.1* between the mouse α-myosin heavy chain promoter and the SV40 polyadenylation sequence of the plasmid (J. Robbins). Each transgene was microinjected into the pronuclei of fertilized C57BL/6J mouse embryos at the single-cell stage. We implanted the embryos into pseudopregnant foster mothers. Positive transgenic mice were identified as described[34]; mice were bred to homozygosity.

Imaging of small mesenteric arteries. Diameter measurement and Ca^{2+} imaging of mouse mesenteric artery were performed as described[48]. Distal mesenteric arteries (2–3 mm length, 120–150 μm passive external diameter) from male C57BL/6J mice were cannulated at both ends and continuously superfused with gassed Krebs solution (37 °C, 70 mmHg) to induce myogenic tone. For measurement of diameter only, the artery outer diameter was continuously monitored by a real-time edge-detection system (National Instruments). For Ca^{2+} imaging, arterial segments were loaded with 15 μM fluo-4-AM for ~3 h. We imaged dye-loaded arteries with a confocal imaging system (Nipkow-Yokogawa dual spinning disk, Solamere Technology) connected to a Nikon Eclipse 2000 microscope equipped with a water immersion objective (×60). Images were captured at the rate of 2–4 frames/s.

Other procedures and materials. Immunoblotting for membrane proteins and immunohistochemistry of frozen sections were performed as described[47,49], with some modifications. We performed analyses of aortic morphology and renal function as described[50]. We also performed measurements of contraction in aortic rings and $[Ca^{2+}]_{cyt}$ (fura-PE3 fluorescence ratio; $R_{340/380}$) in arterial strips as described[34,38], with some modifications (see Supplementary Methods online). We used an unpaired *t*-test, one-way ANOVA followed by Dunnett's test or two-way ANOVA for statistical analyses. Values of $P < 0.05$ were considered statistically significant. SEA0400 (2-[4-[(2,5-difluorophenyl)methoxy]phenoxy]-5-ethoxyaniline) was synthesized by Taisho Pharmaceutical Co. Ltd.

Animal regulations. We used all animals in accordance with the Guidelines for Animal Experiments in Fukuoka University and the US National Institutes of Health Guide for the Care and Use of Laboratory Animals.

Note: Supplementary information is available on the Nature Medicine website.

ACKNOWLEDGMENTS

We thank K. Takahashi and S. Okuyama (Taisho Pharmaceutical Co. Ltd.), K. Saku and H. Urata (Fukuoka University), J. Kimura (Fukushima Medical University) and Y. Matsumura (Osaka University of Pharmaceutical Sciences) for discussions, and W.G. Wier and R. Saunders (University of Maryland) for help in making the video clip. This work was supported by Grants-in-Aid for scientific research (14570097, 16590213) from the Ministry of Education, Science and Culture of Japan, a grant from the Salt Science Research Foundation (No.02), US National Institutes of Health grant HL-45215, and an American Heart Association Mid-Atlantic Affiliate Postdoctoral Fellowship.

COMPETING INTERESTS STATEMENT

The authors declare that they have no competing financial interests.

Received 20 May; accepted 8 September 2004
Published online at http://www.nature.com/naturemedicine/

1. Mosterd, A. *et al.* Trends in the prevalence of hypertension, antihypertensive therapy, and left ventricular hypertrophy from 1950 to 1989. *N. Engl. J. Med.* **340**, 1221–1227 (1999).
2. Kannel, W.B. Elevated systolic blood pressure as a cardiovascular risk factor. *Am. J. Cardiol.* **85**, 251–255 (2000).
3. Cowley, A.W. Long-term control of arterial blood pressure. *Physiol. Rev.* **72**, 231–300 (1992).
4. Blaustein, M.P. Physiological effects of endogenous ouabain: control of intracellular calcium stores and cell responsiveness. *Am. J. Physiol.* **264**, C1367–C1387 (1993).
5. Haddy, F.J. & Pamnani, M.B. Role of dietary salt in hypertension. *J. Am. Coll. Nutr.* **14**, 428–438 (1995).
6. Lifton, R.P., Gharavi, A.G. & Geller, D.S. Molecular mechanisms of human hypertension. *Cell* **104**, 545–556 (2001).
7. Hamlyn, J.M. *et al.* Identification and characterization of a ouabain-like compound from human plasma. *Proc. Natl. Acad. Sci. USA* **88**, 6259–6263 (1991).
8. Schneider, R. *et al.* Bovine adrenals contain, in addition to ouabain, a second inhibitor of the sodium pump. *J. Biol. Chem.* **273**, 784–792 (1998).
9. Bagrov, A.Y. *et al.* Characterization of a urinary bufodienolide Na^+,K^+-ATPase inhibitor in patients after acute myocardial infarction. *Hypertension* **31**, 1097–1103 (1998).
10. Schoner, W. Endogenous cardiac glycosides, a new class of steroid hormones. *Eur. J. Biochem.* **269**, 2440–2448 (2002).
11. Hamlyn, J.M. *et al.* A circulating inhibitor of $(Na^+ + K^+)$-ATPase associated with essential hypertension. *Nature* **300**, 650–652 (1982).
12. Hasegawa, T., Masugi, F., Ogihara, T. & Kumahara, Y. Increase in plasma ouabain-like inhibitor of Na^+,K^+-ATPase with high sodium intake in patients with essential hypertension. *J. Clin. Hypertens.* **3**, 419–429 (1987).
13. Hamlyn, J.M., Hamilton, B.P. & Manunta, P. Endogenous ouabain, sodium balance and blood pressure: a review and a hypothesis. *J. Hypertens.* **14**, 151–167 (1996).

14. Manunta, P. *et al.* Left ventricular mass, stroke volume, and ouabain-like factor in essential hypertension. *Hypertension* **34**, 450–456 (1999).
15. Goto, A. & Yamada, K. Putative roles of ouabainlike compound in hypertension: revisited. *Hypertens. Res.* **23**, S7–S13. (2000).
16. Fedorova, O.V., Lakatta, E.G. & Bagrov, A.Y. Endogenous Na,K pump ligands are differentially regulated during acute NaCl loading of Dahl rats. *Circulation* **102**, 3009–3014 (2000).
17. Ferrari, P. *et al.* PST2238: a new antihypertensive compound that antagonizes the long-term pressor effect of ouabain. *J. Pharmacol. Exp. Ther.* **285**, 83–94 (1998).
18. Takahashi, H. Endogenous digitalislike factor: an update. *Hypertens. Res.* **23**, S1–S5 (2000).
19. Blaustein, M.P. Sodium ions, calcium ions, blood pressure regulation, and hypertension: a reassessment and a hypothesis. *Am. J. Physiol.* **232**, C165–C173 (1977).
20. Philipson, K.D. & Nicoll, D.A. Sodium-calcium exchange: a molecular perspective. *Annu. Rev. Physiol.* **62**, 111–133. (2000).
21. Nakasaki, Y., Iwamoto, T., Hanada, H., Imagawa, T. & Shigekawa, M. Cloning of the rat aortic smooth muscle Na^+/Ca^{2+} exchanger and tissue-specific expression of isoforms. *J. Biochem.* **114**, 528–534 (1993).
22. Lee, S.L., Yu, A.S. & Lytton, J. Tissue-specific expression of Na^+-Ca^{2+} exchanger isoforms. *J. Biol. Chem.* **269**, 14849–14852 (1994).
23. Quednau, B.D., Nicoll, D.A. & Philipson, K.D. Tissue specificity and alternative splicing of the Na^+/Ca^{2+} exchanger isoforms NCX1, NCX2, and NCX3 in rat. *Am. J. Physiol.* **272**, C1250–C1261 (1997).
24. Bers, D.M. Cardiac excitation-contraction coupling. *Nature* **415**, 198–205 (2002).
25. Blaustein, M.P. & Lederer, W.J. Sodium/calcium exchange: its physiological implications. *Physiol. Rev.* **79**, 763–854 (1999).
26. Shigekawa, M. & Iwamoto, T. Cardiac Na^+-Ca^{2+} exchange: molecular and pharmacological aspects. *Circ. Res.* **88**, 864–876 (2001).
27. Matsuda, T. *et al.* SEA0400, a novel and selective inhibitor of the Na^+-Ca^{2+} exchanger, attenuates reperfusion injury in the in vitro and in vivo cerebral ischemic models. *J. Pharmacol. Exp. Ther.* **298**, 249–256 (2001).
28. Iwamoto, T. *et al.* Molecular determinants of Na^+/Ca^{2+} exchange (NCX1) inhibition by SEA0400. *J. Biol. Chem.* **279**, 7544–7553 (2004).
29. Yuan, C.M. *et al.* Long-term ouabain administration produces hypertension in rats. *Hypertension* **22**, 178–187 (1993).
30. Manunta, P., Rogowski, A.C., Hamilton, B.P. & Hamlyn, J.M. Ouabain-induced hypertension in the rat: relationships among plasma and tissue ouabain and blood pressure. *J. Hypertens.* **12**, 549–560 (1994).
31. Berne, R.M. & Levy, M.N. Chapter V. Hemodynamics. in *Cardiovascular Physiology* edn. 8 (eds. Berne, R.M. & Levy, M.N.) 115–134 (Mosby, St. Louis, 2001).
32. Knot, H.J. & Nelson, M.T. Regulation of arterial diameter and wall $[Ca^{2+}]$ in cerebral arteries of rat by membrane potential and intravascular pressure. *J. Physiol.* **508**, 199–209 (1998).
33. Tanaka, H. *et al.* Effect of SEA0400, a novel inhibitor of sodium-calcium exchanger, on myocardial ionic currents. *Br. J. Pharmacol.* **135**, 1096–1100 (2002).
34. Wakimoto, K. *et al.* Targeted disruption of Na^+/Ca^{2+} exchanger gene leads to cardiomyocyte apoptosis and defects in heartbeat. *J. Biol. Chem.* **275**, 36991–36998 (2000).
35. Berridge, M.J., Bootman, M.D. & Roderick, H.L. Calcium signalling: dynamics, homeostasis and remodelling. *Nat. Rev. Mol. Cell Biol.* **4**, 517–529 (2003).
36. Poburko, D., Kuo, K.H., Dai, J., Lee, C.H. & van Breemen, C. Organellar junctions promote targeted Ca^{2+} signaling in smooth muscle: why two membranes are better than one. *Trends Pharmacol. Sci.* **25**, 8–15 (2004).
37. Slodzinski, M.K., Juhaszova, M. & Blaustein, M.P. Antisense inhibition of Na^+/Ca^{2+} exchange in primary cultured arterial myocytes. *Am. J. Physiol.* **269**, C1340–C1345 (1995).
38. Slodzinski, M.K. & Blaustein, M.P. Physiological effects of Na^+/Ca^{2+} exchanger knockdown by antisense oligodeoxynucleotides in arterial myocytes. *Am. J. Physiol.* **275**, C251–C259 (1998).
39. Sweadner, K.J. Isozymes of the Na^+/K^+-ATPase. *Biochim. Biophys. Acta.* **988**, 185–220 (1989).
40. Moore, E.D. *et al.* Coupling of the Na^+/Ca^{2+} exchanger, Na^+/K^+ pump and sarcoplasmic reticulum in smooth muscle. *Nature* **365**, 657–660 (1993).
41. Juhaszova, M. & Blaustein, M.P. Distinct distribution of different Na^+ pump α subunit isoforms in plasmalemma. Physiological implications. *Ann. N.Y. Acad. Sci.* **834**, 524–536 (1997).
42. Fujioka, Y., Matsuoka, S., Ban, T. & Noma, A. Interaction of the Na^+-K^+ pump and Na^+-Ca^{2+} exchange via $[Na^+]_i$ in a restricted space of guinea-pig ventricular cells. *J. Physiol.* **509**, 457–470 (1998).
43. Arnon, A., Hamlyn, J.M. & Blaustein, M.P. Ouabain augments Ca^{2+} transients in arterial smooth muscle without raising cytosolic Na^+. *Am. J. Physiol.* **279**, H679–H691 (2000).
44. Reuter, H. *et al.* The Na^+-Ca^{2+} exchanger is essential for the action of cardiac glycosides. *Circ. Res.* **90**, 305–308 (2002).
45. Aizman, O., Uhlen, P., Lal, M., Brismar, H. & Aperia, A. Ouabain, a steroid hormone that signals with slow calcium oscillations. *Proc. Natl. Acad. Sci. USA* **98**, 13420–13424 (2001).
46. Krushkal, J. *et al.* Genome-wide linkage analyses of systolic blood pressure using highly discordant siblings. *Circulation* **99**, 1407–1410 (1999).
47. Iwamoto, T., Pan, Y., Nakamura, T.Y., Wakabayashi, S. & Shigekawa, M. Protein kinase C-dependent regulation of Na^+/Ca^{2+} exchanger isoforms NCX1 and NCX3 does not require their direct phosphorylation. *Biochemistry* **37**, 17230–17238 (1998).
48. Zhang, J., Wier, W.G. & Blaustein, M.P. Mg^{2+} blocks myogenic tone but not K^+-induced constriction: role for SOCs in small arteries. *Am. J. Physiol.* **283**, H2692–H2705 (2002).
49. Yamashita, J. *et al.* Attenuation of ischemia/reperfusion-induced renal injury in mice deficient in Na^+/Ca^{2+} exchanger. *J. Pharmacol. Exp. Ther.* **304**, 284–293 (2003).
50. Matsumura, Y. *et al.* Exaggerated vascular and renal pathology in endothelin-B receptor-deficient rats with deoxycorticosterone acetate-salt hypertension. *Circulation* **102**, 2765–2773 (2000).

nature medicine

G-CSF prevents cardiac remodeling after myocardial infarction by activating the Jak-Stat pathway in cardiomyocytes

Mutsuo Harada[1,4], Yingjie Qin[1,4], Hiroyuki Takano[1,4], Tohru Minamino[1,4], Yunzeng Zou[1], Haruhiro Toko[1], Masashi Ohtsuka[1], Katsuhisa Matsuura[1], Masanori Sano[1], Jun-ichiro Nishi[1], Koji Iwanaga[1], Hiroshi Akazawa[1], Takeshige Kunieda[1], Weidong Zhu[1], Hiroshi Hasegawa[1], Keita Kunisada[2], Toshio Nagai[1], Haruaki Nakaya[3], Keiko Yamauchi-Takihara[2] & Issei Komuro[1]

Granulocyte colony-stimulating factor (G-CSF) was reported to induce myocardial regeneration by promoting mobilization of bone marrow stem cells to the injured heart after myocardial infarction, but the precise mechanisms of the beneficial effects of G-CSF are not fully understood. Here we show that G-CSF acts directly on cardiomyocytes and promotes their survival after myocardial infarction. G-CSF receptor was expressed on cardiomyocytes and G-CSF activated the Jak/Stat pathway in cardiomyocytes. The G-CSF treatment did not affect initial infarct size at 3 d but improved cardiac function as early as 1 week after myocardial infarction. Moreover, the beneficial effects of G-CSF on cardiac function were reduced by delayed start of the treatment. G-CSF induced antiapoptotic proteins and inhibited apoptotic death of cardiomyocytes in the infarcted hearts. G-CSF also reduced apoptosis of endothelial cells and increased vascularization in the infarcted hearts, further protecting against ischemic injury. All these effects of G-CSF on infarcted hearts were abolished by overexpression of a dominant-negative mutant Stat3 protein in cardiomyocytes. These results suggest that G-CSF promotes survival of cardiac myocytes and prevents left ventricular remodeling after myocardial infarction through the functional communication between cardiomyocytes and noncardiomyocytes.

Myocardial infarction is the most common cause of cardiac morbidity and mortality in many countries, and left ventricular remodeling after myocardial infarction is important because it causes progression to heart failure. Several cytokines including G-CSF, erythropoietin and leukemia inhibitory factor have beneficial effects on cardiac remodeling after myocardial infarction[1–5]. In particular, G-CSF markedly improves cardiac function and reduce mortality after myocardial infarction in mice, possibly by regeneration of myocardium and angiogenesis[1,2,6–8]. G-CSF is known to have various functions such as induction of proliferation, survival and differentiation of hematopoietic cells, as well as mobilization of bone marrow cells[9–11]. Although it was reported that bone marrow cells could differentiate into cardiomyocytes and vascular cells, thereby contributing to regeneration of myocardium and angiogenesis in ischemic hearts[12–15], accumulating evidence has questioned these previous reports[16–18]. In this study, we examined the molecular mechanisms of how G-CSF prevents left ventricular remodeling after myocardial infarction.

RESULTS

G-CSF directly acts on cultured cardiomyocytes

G-CSF receptor (G-CSFR, encoded by *CSF3R*) has been reported to be expressed only on blood cells such as myeloid leukemic cells, leukemic cell lines, mature neutrophils, platelets, monocytes and some lymphoid cell lines[9]. To test whether G-CSFR is expressed on mouse cardiomyocytes, we performed a reverse transcription–polymerase chain reaction (RT-PCR) experiment by using specific primers for mouse *Csf3r*. We detected expression of the *Csf3r* gene in the adult mouse heart and cultured neonatal cardiomyocytes (**Fig. 1a**). We next examined expression of G-CSFR protein in cultured cardiomyocytes of neonatal rats by immunocytochemistry. Similar to the previously reported expression pattern of G-CSFR in living cells[19], the immunoreactivity for G-CSFR was localized to the cytoplasm and cell membrane under steady-state conditions in cardiomyocytes (**Fig. 1b**). This immunoreactivity disappeared when the antibody specific for G-CSFR was omitted, validating its specificity (**Fig. 1b**). In addition to cardiomyocytes, we also detected expression of G-CSFR on cardiac fibroblasts by immunocytochemistry (see **Supplementary Fig. 1** online) and RT-PCR (**Supplementary Fig. 2** online).

The binding of G-CSF to its receptor has been reported to evoke signal transduction by activating the receptor-associated Janus family tyrosine kinases (JAK) and signal transducer and activator of transcription (STAT) proteins in hematopoietic cells[9,10]. In particular, STAT3

[1]Department of Cardiovascular Science and Medicine, Chiba University Graduate School of Medicine, 1-8-1 Inohana, Chuo-ku, Chiba 260-8670, Japan. [2]Department of Molecular Medicine, Osaka University Medical School, Osaka University, 2-2 Yamadaoka, Suita, Osaka 565-0871, Japan. [3]Department of Pharmacology, Chiba University Graduate School of Medicine, 1-8-1 Inohana, Chuo-ku, Chiba 260-8670, Japan. [4]These authors contributed equally to this work. Correspondence should be addressed to I.K. (komuro-tky@umin.ac.jp).

Published online 20 February 2005; doi:10.1038/nm1199

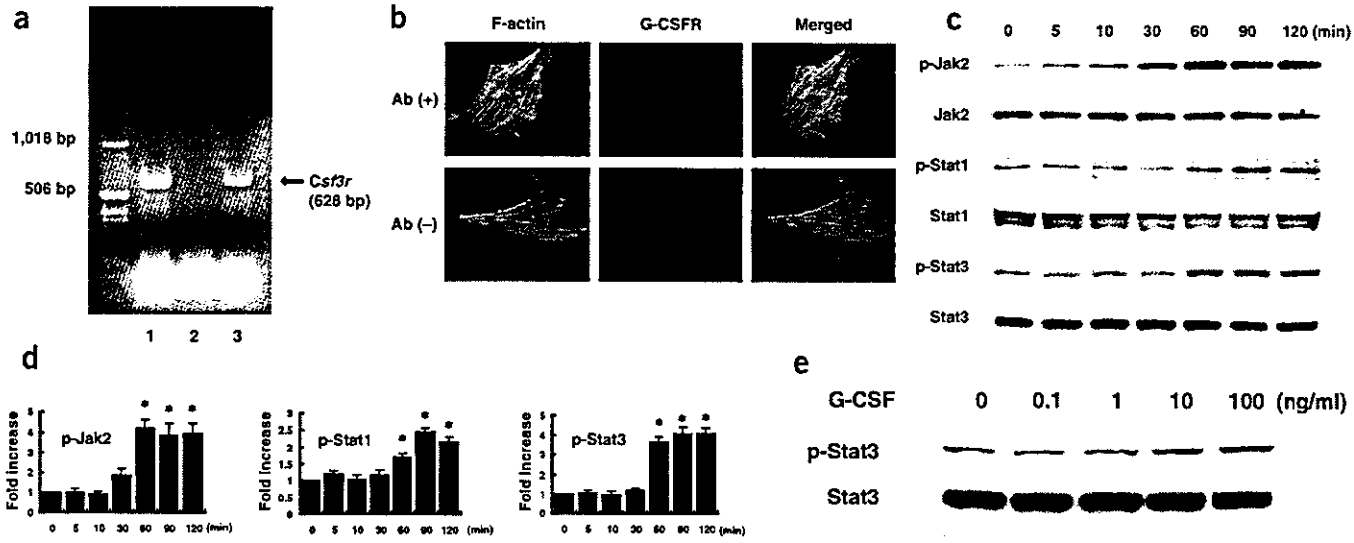

Figure 1 Expression of G-CSFR and the G-CSF-evoked signal transduction in cultured cardiomyocytes. (**a**) RT-PCR for mouse *Csf3r*. Expression of *Csf3r* was detected in the adult mouse heart (lane 1) and cultured cardiomyocytes of neonatal mice (lane 3). In lane 2, reverse transcription products were omitted to exclude the possibility of false-positive results from contamination. (**b**) Immunocytochemical staining for G-CSFR. Cardiomyocytes from neonatal rats were incubated with antibody to G-CSFR (red) and phalloidin (green) (upper panel). In the absence of antibody to G-CSFR, no signal was detected (lower panel). Original magnification, ×1,000. (**c**) G-CSF induces phosphorylation of Jak2, Stat1 and Stat3 in a time-dependent manner in cultured cardiomyocytes. (**d**) Quantification of Jak2, Stat1 and Stat3 activation by G-CSF stimulation as compared with control (time = 0). $^*P < 0.05$ versus control ($n = 3$). (**e**) G-CSF induces phosphorylation and activation of Stat3 in a dose-dependent manner in cultured cardiomyocytes.

has been reported to contribute to G-CSF-induced myeloid differentiation and survival[20,21]. We therefore examined whether G-CSF activates the Jak-Stat signaling pathway in cultured cardiomyocytes. G-CSF (100 ng/ml) significantly induced phosphorylation and activation of Jak2 and Stat3, and to a lesser extent, Stat1 but not Jak1, Tyk2 or Stat5 in a dose-dependent manner (Fig. 1c–e and data not shown), suggesting that G-CSFR on cardiomyocytes is functional.

We next examined whether G-CSF confers direct protective effects on cardiomyocytes as it prevents hematopoietic cells from apoptotic death[21]. We exposed cardiomyocytes to 0.1 mM H_2O_2 in the absence or presence of G-CSF and examined cardiomyocyte apoptosis by staining with annexin V[22,23]. Pretreatment with G-CSF significantly reduced the number of H_2O_2-induced annexin V–positive cells compared with cells that were not given the G-CSF pretreatment

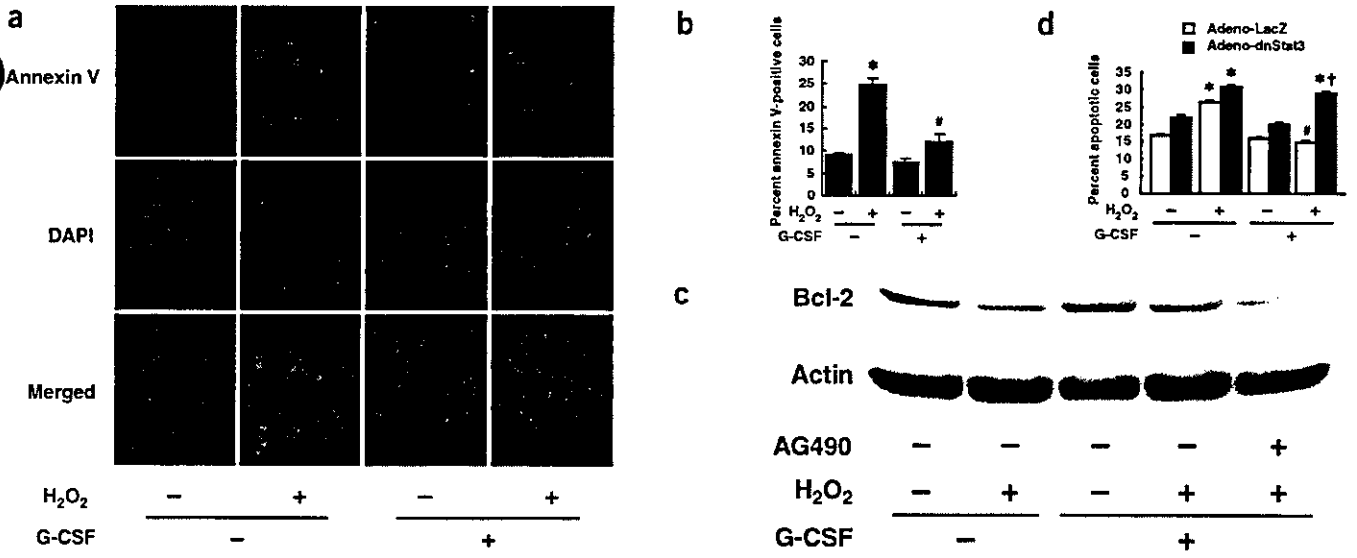

Figure 2 Suppression of H_2O_2-induced cardiomyocyte apoptosis by G-CSF. (**a**) Detection of apoptosis by Cy3-labeled annexin V. Red fluorescence shows apoptotic cardiomyocytes stained with Cy3-labeled annexin V. Nuclei were counterstained with DAPI staining (blue). Original magnification, ×400. (**b**) Quantitative analysis of apoptotic cells. The vertical axis indicates the ratio of the annexin V–positive cell number relative to that of DAPI-positive nuclei. $^*P < 0.01$ versus nontreated cells, $^\#P < 0.05$ versus H_2O_2-treated cells without G-CSF ($n = 3$). (**c**) G-CSF prevents H_2O_2-induced downregulation of Bcl-2 expression ($n = 3$). (**d**) Inhibition of antiapoptotic effects of G-CSF by Adeno-dnStat3. Bar graphs represent quantitative analysis of the apoptotic cell number relative to the total cell number. $^*P < 0.001$ versus H_2O_2 (–)/G-CSF (–), $^\#P < 0.001$ versus H_2O_2 (+)/G-CSF (–), $^\dagger P < 0.001$ versus H_2O_2 (+)/G-CSF (+)/Adeno-LacZ ($n = 3$).

(Fig. 2a,b). To investigate the molecular mechanism of how G-CSF exerts an antiapoptotic effect on cultured cardiomyocytes, we examined expression of the Bcl-2 protein family, known target molecules of the Jak-Stat pathway[24], by western blot analysis. Expression levels of antiapoptotic proteins such as Bcl-2 and Bcl-xL were lower when cardiomyocytes were subjected to H_2O_2 (Fig. 2c and data not shown), and this reduction was considerably inhibited by G-CSF pretreatment (Fig. 2c). AG490, an inhibitor of Jak2, abolished G-CSF-induced Bcl-2 expression (Fig. 2c) but did not affect its basal levels (**Supplementary Fig. 3** online), suggesting a crucial role of the Jak-Stat pathway in inducing survival of cardiomyocytes by G-CSF. To further elucidate the involvement of the Jak-Stat pathway in the protective effects of G-CSF on cardiomyocytes, we transduced cultured cardiomyocytes with adenovirus encoding dominant-negative Stat3 (Adeno-dnStat3). G-CSF treatment significantly reduced apoptosis induced by H_2O_2 in Adeno-LacZ-infected cardiomyocytes (**Fig. 2d**). This effect was abolished by introduction of Adeno-dnStat3 (**Fig. 2d**), suggesting that Stat3 mediates the protective effects of G-CSF on H_2O_2-induced cardiomyocyte apoptosis.

Effects of G-CSF on cardiac function after myocardial infarction

Consistent with the *in vitro* data, G-CSF enhanced activation of Stat3 in the infarcted heart (**Fig. 3a**). Notably, the levels of G-CSFR were markedly increased after myocardial infarction in cardiomyocytes (**Supplementary Fig. 4** online), which may enhance the effects of G-CSF on the infarcted heart. To elucidate the role of G-CSF-induced Stat3 activation in cardiac remodeling, we produced myocardial infarction in transgenic mice which express dominant-negative Stat3 in cardiomyocytes under the control of the α-myosin heavy chain promoter (dnStat3-Tg). Administration of G-CSF was started at the time of coronary artery ligation (day 0) until day 4 in transgenic mice; we termed this group Tg-G mice. A control group of dnStat3-Tg mice given myocardial infarction received saline (Tg-cont) instead of G-CSF. We also included two groups of wild-type mice given myocardial infarction treated with G-CSF (Wt-G) or saline (Wt-cont). At 2 weeks after myocardial infarction, we assessed the morphology by histological analysis and measured cardiac function by echocardiography and catheterization analysis. The infarct area was significantly smaller in the Wt-G group than the Wt-cont group (**Fig. 3b**). The Wt-G group also showed less left ventricular end-diastolic dimension (LVEDD) and better fractional shortening as assessed by echocardiography, and lower end-diastolic pressure (LVEDP) and better $+dp/dt$ and $-dp/dt$ as assessed by cardiac catheterization compared with Wt-cont (**Fig. 3c**). The beneficial effects of G-CSF on cardiac function were dose dependent and were significantly reduced by delayed start of the treatment (**Fig. 3d,e** and **Supplementary Fig. 5** online). Moreover, its favorable effects on cardiac function became evident within 1 week after the treatment (**Fig. 3f**). Disruption of the Stat3 signaling pathway in cardiomyocytes abolished the protective effects of G-CSF. There was no significant difference in LVEDD, fractional shortening, LVEDP, $+dp/dt$ and $-dp/dt$ between Tg-G and Tg-cont (**Fig. 3c**). We obtained similar results from infarcted female hearts (**Fig. 3g**). These results suggest that G-CSF protects the heart after myocardial infarction at least in part by directly activating Stat3 in cardiomyocytes, which is a gender-independent effect. We have previously shown that treatment with G-CSF significantly ($P < 0.05$) decreased myocardial infarction–related mortality of wild-type mice[2]. In contrast, there were no significant differences in mortality between G-CSF-treated and saline-treated dnStat3-Tg mice (data not shown).

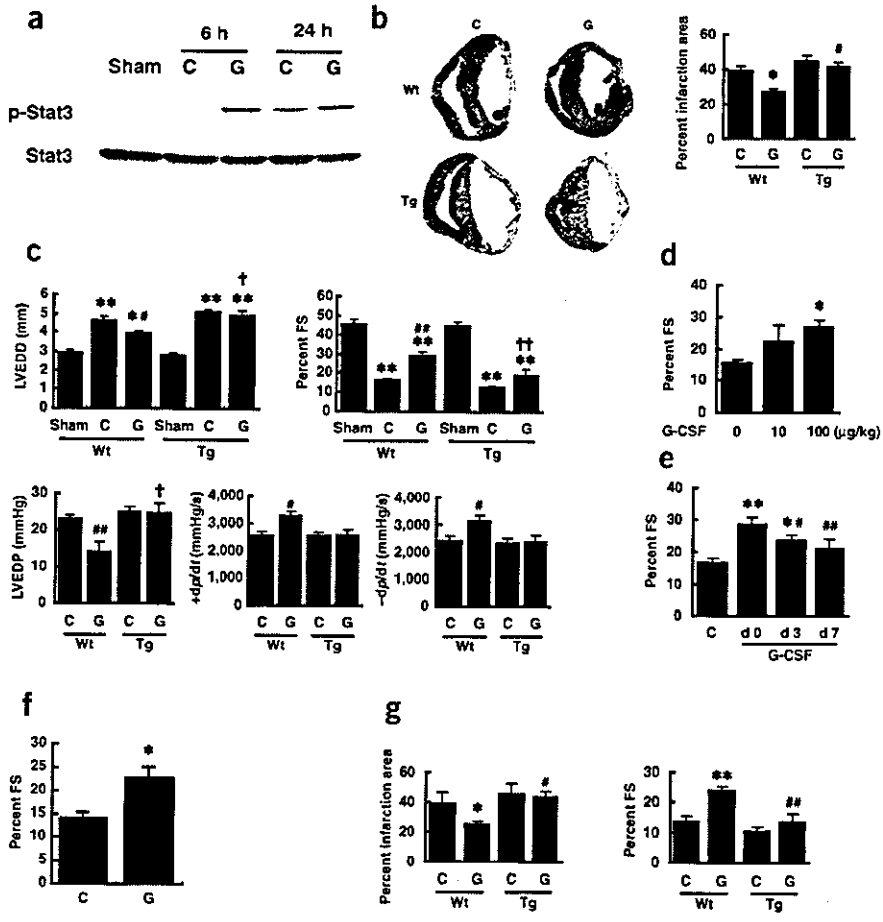

Figure 3 Effects of G-CSF on cardiac function after myocardial infarction. (**a**) Stat3 activation in the infarcted hearts. We operated on wild-type mice to induce myocardial infarction and treated them with G-CSF (G) or saline (C). (**b**) Masson trichrome staining of wild-type (Wt) and dnStat3-Tg (Tg) hearts. $^{*}P < 0.001$ versus Wt-cont, $^{\#}P < 0.001$ versus Wt-G ($n = 11$–15). (**c**) G-CSF treatment preserves cardiac function after myocardial infarction. $^{*}P < 0.01$, $^{**}P < 0.001$ versus sham; $^{\#}P < 0.05$, $^{\#\#}P < 0.001$ versus Wt-cont; $^{\dagger}P < 0.01$, $^{\dagger\dagger}P < 0.001$ versus Wt-G ($n = 10$–15 for echocardiography and $n = 5$ for catheterization analysis). (**d**) Dose-dependent effects of G-CSF. FS, fractional shortening. $^{*}P < 0.01$ versus saline-treated mice (G-CSF = 0)($n = 12$–14). (**e**) Wild-type mice were operated to induce myocardial infarction and G-CSF treatment (100 μg/kg/d) was started from the indicated day for 5 d. $^{*}P < 0.05$, $^{**}P < 0.001$ versus saline-treated mice (C); $^{\#}P < 0.05$, $^{\#\#}P < 0.01$ versus mice treated at day 0 (d 0) ($n = 11$–12). (**f**) Effects of G-CSF on cardiac function at 1 week. $^{*}P < 0.05$ versus control ($n = 3$). (**g**) Effects of G-CSF on cardiac function of female mice. $^{*}P < 0.05$, $^{**}P < 0.001$ versus Wt-cont; $^{\#}P < 0.05$, $^{\#\#}P < 0.005$ versus Wt-G ($n = 4$–5).

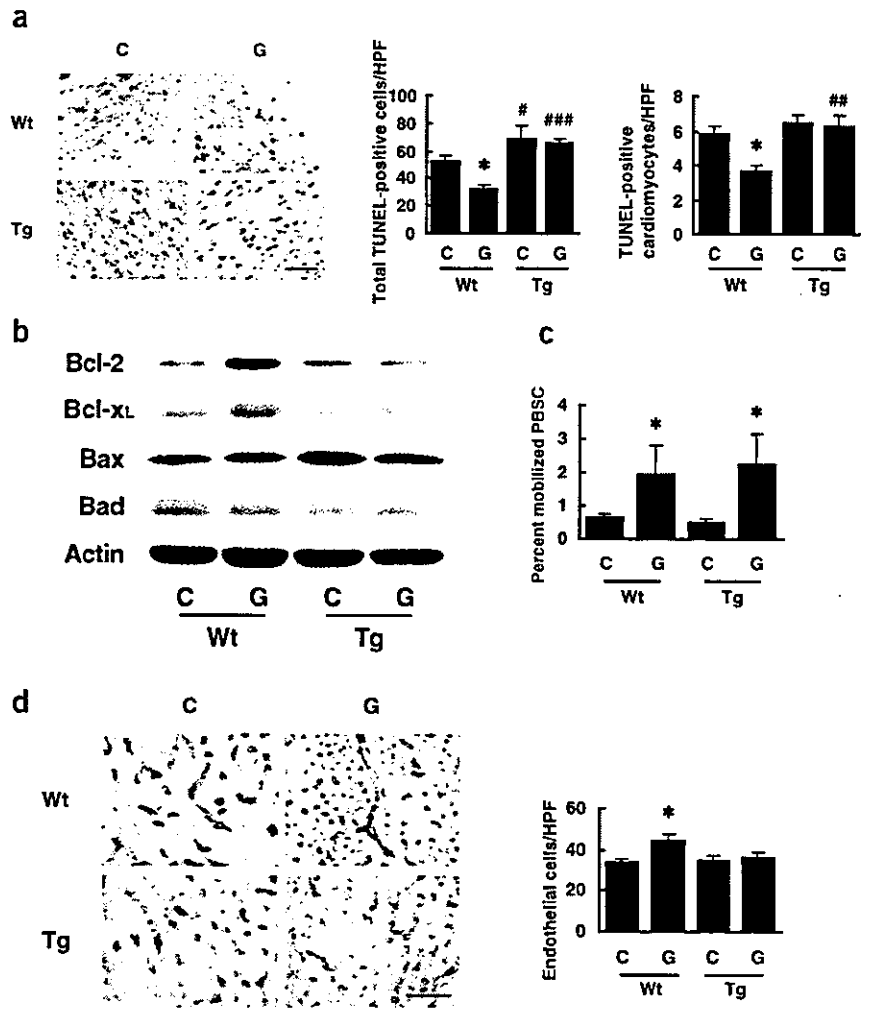

Figure 4 Mechanisms of the protective effects of G-CSF. (a) TUNEL staining (brown nuclei) in the infarcted hearts. The graphs show quantitative analyses for total TUNEL-positive cells (left graph) and TUNEL-positive cardiomyocytes (right graph) in infarcted hearts. $^{*}P < 0.01$ versus Wt-cont; $^{\#}P < 0.05$, $^{\#\#}P < 0.005$, $^{\#\#\#}P < 0.001$ versus wild-type mice with the same treatment ($n = 5$–7). Scale bar, 100 μm. (b) Infarcted hearts treated with G-CSF (G) or saline (C) were analyzed for expression of Bcl-2, Bcl-xL, Bax and Bad by western blotting ($n = 3$). (c) Mobilization of hematopoietic stem cells into peripheral blood (PBSC). $^{*}P < 0.05$ versus saline-treated mice ($n = 4$). (d) Capillary endothelial cells were identified by immunohistochemical staining with anti-PECAM antibody in the border zone of the infarcted hearts. Scale bar, 100 μm. The number of endothelial cells was counted and shown in the graph ($n = 6$–8). $^{*}P < 0.05$.

Mechanisms of the protective effects of G-CSF

Our *in vitro* results suggest that the protective effects of G-CSF on cardiac remodeling after myocardial infarction can be attributed in part to reduction of cardiomyocyte apoptosis. To determine whether the Stat3 pathway in cardiomyocytes mediates the antiapoptotic effects of G-CSF on the ischemic myocardium, we carried out TUNEL labeling of left ventricular sections 24 h after myocardial infarction in wild-type mice and dnStat3-Tg mice. Although the number of TUNEL-positive cells was significantly less in the Wt-G group than the Wt-cont group, G-CSF treatment had no effect on cardiomyocyte apoptosis in dnStat3-Tg mice (**Fig. 4a**). The effects of G-CSF on apoptosis after myocardial infarction were also attenuated when mice were treated with AG490 (**Supplementary Fig. 6** online). Myocardial infarction–related apoptosis was significantly increased in the Tg-cont group and AG490-treated wild-type mice compared with Wt-cont mice (**Fig. 4a** and **Supplementary Fig. 6** online), suggesting that endogenous activation of Stat3 has a protective role in the infarcted heart, as reported previously[25]. It is noteworthy that G-CSF treatment inhibited apoptosis of noncardiomyocytes including endothelial cells and that this inhibition was abolished in dnStat3-Tg mice (**Fig. 4a** and data not shown). To investigate the underlying molecular mechanism of the antiapoptotic effects of G-CSF *in vivo*, we examined expression of the Bcl-2 protein family by western blot analysis. Consistent with our *in vitro* results, expression of antiapoptotic proteins such as Bcl-2 and Bcl-xL was significantly increased in the Wt-G group at 24 h after myocardial infarction compared with the Wt-cont group, whereas expression of the proapoptotic proteins Bax and Bad was not affected by the treatment (**Fig. 4b**). In contrast, expression levels of antiapoptotic proteins were not increased by G-CSF in the Tg-G group (**Fig. 4b**). Immunohistochemical analysis also showed increased expression of Bcl-2 in the infarcted heart of the Wt-G group but not of the Tg-G group (**Supplementary Fig. 7** online).

To determine the effects of G-CSF on mobilization of stem cells, we counted the number of cells positive for both Sca-1 and c-kit in peripheral blood samples from mice treated with G-CSF or saline. The G-CSF treatment similarly increased the number of double-positive cells in wild-type mice and dnStat3-Tg mice (**Fig. 4c**). To examine the impact of G-CSF on cardiac homing of bone marrow cells, we transplanted bone marrow cells derived from GFP transgenic mice into wild-type and dnStat3-Tg mice, produced myocardial infarction and treated with G-CSF or saline. FACS analysis showed that G-CSF did not increase cardiac homing of bone marrow cells in wild-type and dnStat3-Tg mice (**Supplementary Fig. 8** online). We have shown that cardiac stem cells, which are able to differentiate into cardiomyocytes, exist in Sca-1-positive populations in the adult myocardium[26]. But G-CSF treatment did not affect the number of Sca-1-positive cells in the infarcted hearts of wild-type or dnStat3-Tg mice (**Supplementary Fig. 9** online). Thus, it is unlikely that G-CSF exerts its beneficial effects through expansion of cardiac stem cells. To determine the effects of G-CSF on proliferation of cardiomyocytes, we carried out immunostaining for Ki67, a marker for cell cycling, in conjunction with a labeling for troponin T. The number of Ki67-positive cardiomyocytes was increased in the infarcted hearts of wild-type mice and dnStat3-Tg mice compared with sham-operated mice (**Supplementary Fig. 10** online). But G-CSF did not alter the number of Ki67-positive cardiomyocytes in wild-type or dnStat3-Tg mice, suggesting that G-CSF does not induce proliferation of cardiomyocytes (**Supplementary Fig. 10** online). The number of Ki67-positive cardiomyocytes was less in infarcted hearts of dnStat3-Tg mice than in those of wild-type mice, suggesting that endogenous Stat3 activity is required

for myocardial regeneration after myocardial infarction and that activation of Stat3 by G-CSF is not sufficient for cardiomyocytes to enter the cell cycle in infarcted hearts of wild-type mice (**Supplementary Fig. 10** online). In contrast, G-CSF treatment significantly increased the number of endothelial cells in the border zone of the infarcted hearts (**Fig. 4d**). This increase was attenuated in dnStat3-Tg mice, indicating that the increased vascularity is mediated by Stat3 activity in cardiomyocytes and may partially account for the beneficial effects of G-CSF on the infarcted hearts. Taken together with the result that G-CSF-induced inhibition of noncardiomyocyte apoptosis was also mediated by the Stat3 signaling pathway in cardiomyocytes (**Fig. 4a**), these findings imply that communication between cardiomyocytes and noncardiomyocytes regulates each others' survival.

To further test whether G-CSF acts directly on the heart, we examined the effects of G-CSF treatment on cardiac function after ischemia-reperfusion injury in a Langendorff perfusion model. The isolated hearts underwent 30 min total ischemia followed by 120 min reperfusion with the perfusate containing G-CSF (300 ng/ml) or vehicle, and left ventricular developed pressure (LVDP, measured as the difference between systolic and diastolic pressures of the left ventricle) and LVEDP were measured. There were no significant differences in basal hemodynamic parameters including heart rate, left ventricular pressure, LVEDP and positive and negative d*p*/d*t*, between the control group and G-CSF group (**Table 1**). After reperfusion, however, G-CSF-treated hearts started to beat earlier than those of the control group (**Fig. 5a**). At 120 min after reperfusion, contractile function (LVDP) of G-CSF-treated hearts was significantly better than that of control hearts (**Fig. 5a**). Likewise, diastolic function (LVEDP) of G-CSF-treated hearts was better than that of control hearts (**Fig. 5a**). After ischemia-reperfusion, there was more viable myocardium (red lesion) in G-CSF-treated hearts than control hearts (**Fig. 5b**). The size of the infarct (white lesion) was significantly smaller in G-CSF-treated hearts than in control hearts (**Fig. 5b**).

Table 1 Basal hemodynamic parameters

	Control ($n = 7$)	G-CSF ($n = 7$)
HR (b.p.m.)	326 ± 34	334 ± 24
LVP (mmHg)	121.8 ± 24	117.3 ± 32
LVEDP (mmHg)	4.3 ± 1.3	4.5 ± 1.6
+d*p*/d*t* (mmHg/s)	7,554 ± 643	7,657 ± 377
–d*p*/d*t* (mmHg/s)	6,504 ± 638	6,670 ± 602

HR, heart rate; b.p.m., beats per minute; LVP, left ventricular pressure; LVEDP, left ventricular end-diastolic pressure; +d*p*/d*t* and –d*p*/d*t*, positive and negative first derivatives for maximal rates of left ventricular pressure development.

DISCUSSION

In the present study, G-CSFR was found to be expressed on cardiomyocytes and cardiac fibroblasts, and G-CSF activated Jak2 and the downstream signaling molecule Stat3 in cultured cardiomyocytes. Treatment with G-CSF protected cultured cardiomyocytes from apoptotic cell death possibly through upregulation of Bcl-2 and Bcl-xL expression, suggesting that G-CSF has direct protective effects on cardiomyocytes through G-CSFR and the Jak-Stat pathway. This idea is further supported by the *in vivo* experiments. G-CSF enhanced Stat3 activity and increased expression of Bcl-2 and Bcl-xL in the infarcted heart where G-CSFR was markedly upregulated, thereby preventing cardiomyocyte apoptosis and cardiac dysfunction. These effects of G-CSF were abolished when Stat3 activation was disrupted in cardiomyocytes, suggesting that a direct action of G-CSF on cardiomyocytes has a crucial role in preventing left ventricular remodeling after myocardial infarction. Because noncardiomyocytes also expressed G-CSFR, the possibility exists that activation of G-CSF receptors on these cells modulates the beneficial effects of G-CSF on infarcted hearts.

The mobilization of bone marrow stem cells (BMSC) to the myocardium has been considered to be the main mechanism by which G-CSF ameliorates cardiac remodeling after myocardial infarction[1,6–8]. In this study, we showed that G-CSF reduces apoptotic cell death and effectively protects the infarcted heart, which is dependent on its direct action on cardiomyocytes through the Stat3 pathway. This antiapoptotic mechanism seems to be more important than induction of BMSC mobilization, because disruption of

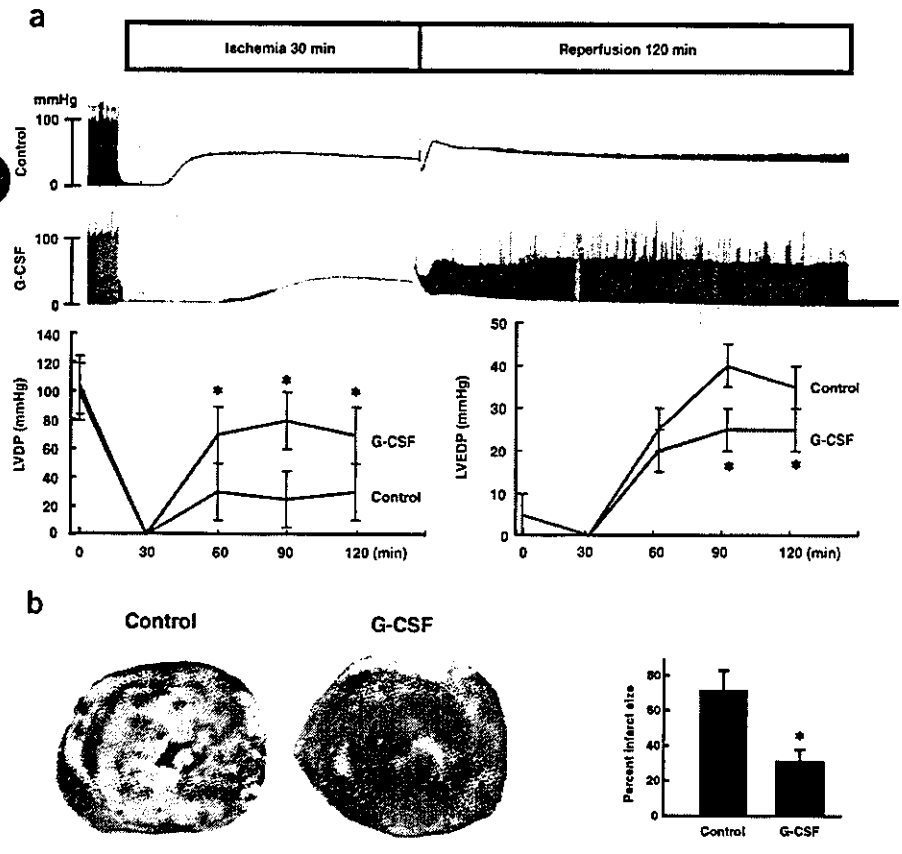

Figure 5 Direct effects of G-CSF on cardiac function after ischemia-reperfusion injury. (a) Representative left ventricular pressure records of control and G-CSF-treated hearts are shown (upper panel). The graphs show changes in LVDP (left) and LVEDP (right) during ischemia-reperfusion. *$P < 0.05$ versus control hearts ($n = 7$). (b) The photographs show representative TTC staining of control hearts (Control) and G-CSF-treated hearts (G-CSF) after ischemia-reperfusion. The graph indicates myocardial infarct sizes for control hearts (Control) and G-CSF-treated hearts (G-CSF). Infarct sizes were calculated as described in **Supplementary Methods** online. *$P < 0.05$ versus control hearts ($n = 7$).

this pathway by expressing dnStat3 in cardiomyocytes almost abolished the protective effects of G-CSF on cardiac remodeling after myocardial infarction. In addition, there was no difference in the effects of G-CSF on mobilization and cardiac homing of bone marrow cells, expansion of cardiac stem cells, and proliferation of cardiomyocytes between wild-type and dnStat3-Tg mice. The beneficial effects of G-CSF and stem cell factor on the infarcted heart has been described, but no evidence indicating that G-CSF induced cardiac homing of bone marrow cells in the infarcted heart has been shown[1]. In this study, we found favorable effects of G-CSF on the infarcted heart as early as 1 week after the treatment even though cardiac homing of bone marrow cells was not increased. Thus, we conclude that increased cardiac homing of bone marrow cells cannot account for improved function of the infarcted heart after G-CSF treatment.

The JAK-STAT pathway has been shown to induce various angiogenic factors besides antiapoptotic proteins[20,21]. The number of endothelial cells in the border zone was increased by G-CSF through Stat3 activation in cardiomyocytes. Consistent with this, we noted that G-CSF induces cardiac expression of angiogenic factors *in vitro* and *in vivo*, which appears to be mediated by cardiac Stat3 activation (M.H., Y.Q., H.T., T.M. & I.K., unpublished data). Moreover, we observed that the majority of apoptotic cells in the infarcted hearts was endothelial cells and that endothelial apoptosis was significantly inhibited by G-CSF treatment in wild-type mice but not in dnStat3-Tg mice (**Fig. 4a** and M.H., T.M. & I.K., unpublished data). Thus, activation of this pathway in cardiomyocytes by G-CSF may also promote angiogenesis and protect against endothelial apoptosis by producing angiogenic factors, resulting in the further prevention of cell death of cardiomyocytes and cardiac remodeling after myocardial infarction. The results in this study provide new mechanistic insights of the G-CSF therapy on infarcted hearts.

METHODS

For further details, please see **Supplementary Methods** online.

Cell culture. Cardiomyocytes prepared from ventricles of 1-d-old Wistar rats[27] were plated onto 60-mm plastic culture dishes at a concentration of 1×10^5 cells/cm^2 and cultured in Dulbecco modified Eagle medium (DMEM) supplemented with 10% fetal bovine serum (FBS) at 37 °C in a mixture of 95% air and 5% CO_2. The culture medium was changed to serum-free DMEM 24 h before stimulation. Generation and infection of recombinant adenovirus were performed as described[28].

Percoll enrichment of adult mouse cardiomyocytes and noncardiomyocytes. Adult mouse cardiomyocytes were prepared from 10-week-old C57BL/6 male mice according to the Alliance for Cellular Signaling protocol. We also prepared cardiomyocytes and noncardiomyocytes from myocardial infarction-operated or sham-operated C57BL/6 male mice. After digestion, cells were dissociated, resuspended in differentiation medium and loaded onto a discontinuous Percoll gradient. Cardiomyocytes or noncardiomyocytes were separately collected as described previously[29] and subsequently washed with 1 × phosphate-buffered saline for RT-PCR.

RNA extraction and RT-PCR analysis. Total RNA from adult mice cardiomyocytes was isolated by the guanidinium thiocyanate-phenol chloroform method. A total of 4 μg RNA was transcribed with MMLV reverse transcriptase and random hexamers. The cDNA was amplified using a mouse *Csf3r* exon 15 forward primer (5′-GTACTCTTGTCCACTACCTGT-3′) and an exon 17 reverse primer (5′-CAAGATACAAGGACCCCCAA-3′). We performed PCR under the following conditions: an initial denaturation at 94 °C for 2 min followed by a cycle of denaturation at 94 °C for 1 min, annealing at 58 °C for 1 min and extension at 72 °C for 1 min. We subjected samples to 40 cycles followed by a final extension at 72 °C for 3 min. The products were analyzed on a 1.5% ethidium bromide stained agarose gel.

Immunocytochemistry. Cardiomyocytes or noncardiomyocytes of neonatal rats cultured on glass cover slips were incubated with or without the antibody to G-CSFR (Santa Cruz Biotechnology) for 1 h, followed by incubation with Cy3-labeled secondary antibodies. After washing, we double-stained the cells with fluorescent phalloidin (Molecular Probes) for 1 h at room temperature.

Western blots. Western blot analysis was performed as described[5]. We probed the membranes with antibodies to phospho-Jak2, phospho-Stat3 (Cell Signaling), phospho-Jak1, phospho-Tyk2, phospho-Stat1, phospho-Stat5, anti-Jak1, Jak2, Tyk2, Stat1, Stat3, Stat5, Bcl-2, Bax, G-CSFR (Santa Cruz Biotechnology), Bcl-xL, Bad (Transduction Laboratories) or actin (Sigma-Aldrich). We used the ECL system (Amersham Biosciences Corp) for detection.

Animals and surgical procedures. Generation and genotyping of dnStat3-Tg mice have been previously described[28]. All mice used in this study were 8–10-week-old males, unless indicated. All experimental procedures were performed according to the guidelines established by Chiba University for experiments in animals and all protocols were approved by our institutional review board. We anesthetized mice by intraperitoneally injecting a mixture of 100 mg/kg ketamine and 5 mg/kg xylazine. Myocardial infarction was produced by ligation of the left anterior descending artery. We operated on dnStat3-Tg mice to induce myocardial infarction and randomly divided them into two groups, the G-CSF-treated group (10–100 μg/kg/d subcutaneously for 5 d consecutively, Kyowa Hakko Kogyo Co.) and the saline-treated group. We operated on nontransgenic mice as control groups using the same procedures and divided them into a G-CSF-treated group and a saline-treated group. Some mice were randomly chosen to be analyzed for initial area at risk by injection of Evans blue dye after producing myocardial infarction. There was no difference in initial area sizes at risk between saline-treated control and G-CSF-treated mice ($n = 5$; **Supplementary Fig. 11** online). We also determined initial infarct size by triphenyltetrazolium chloride staining on day 3. There was no significant difference in initial infarct size between saline-treated control and G-CSF-treated mice ($n = 5$; **Supplementary Fig. 12** online).

Echocardiography and catheterization. Transthoracic echocardiography was performed with an Agilent Sonos 4500 (Agilent Technology Co.) provided with an 11-MHz imaging transducer. For catheterization analysis, the right carotid artery was cannulated under anesthesia by the micro pressure transducers with an outer diameter of 0.42 mm (Samba 3000; Samba Sensors AB), which was then advanced into the left ventricle. Pressure signals were recorded using a MacLab 3.6/s data acquisition system (AD Instruments) with a sampling rate of 2,000 Hz. Mice were anesthetized as described above, and heart rate was kept at approximately 270–300 beats per minute to minimize data deviation when we measured cardiac function.

Histology. Hearts fixed in 10% formalin were embedded in paraffin, sectioned at 4 μm thickness, and stained with Masson trichrome. The extent of fibrosis was measured in three sections from each heart and the value was expressed as the ratio of Masson trichrome stained area to total left ventricular free wall. For apoptosis analysis, infarcted hearts were frozen in cryomolds, sectioned, and TUNEL labeling was performed according to the manufacturer's protocol (*In Situ* Apoptosis Detection kit; Takara) in combination with immunostainings for appropriate cell markers. Digital photographs were taken at magnification ×400, and 25 random high-power fields (HPF) from each heart sample were chosen and quantified in a blinded manner. We examined vascularization by measuring the number of capillary endothelial cells in light-microscopic sections taken from the border zone of the hearts 2 weeks after myocardial infarction. Capillary endothelial cells were identified by immunohistochemical staining with antibody to platelet endothelial cell adhesion molecule (PECAM; Pharmingen). Ten random microscopic fields in the border zone were examined and the number of endothelial cells was expressed as the number of PECAM-positive cells/HPF (magnification, ×400).

Statistical analysis. Data are shown as mean ± s.e.m. Multiple group comparison was performed by one-way analysis of variance (ANOVA) followed by the Bonferroni procedure for comparison of means. Comparison between two groups were analyzed by the two-tailed Student's *t*-test or two-way ANOVA. Values of $P < 0.05$ were considered statistically significant.

URL. Alliance for Cellular Signaling Procedure Protocols
http://www.signaling-gateway.org/data/cgi-bin/Protocols.cgi?cat=0

Note: Supplementary information is available on the Nature Medicine website.

ACKNOWLEDGMENTS

The authors thank J. Robbins (Children's Hospital Research Foundation, Cincinnati, Ohio) for a fragment of the αMHC gene promoter, M. Tamagawa for the analysis of Langendorff-perfused model, Kirin Brewery Co., Ltd. for their kind gift of G-CSF, and M. Watanabe and E. Fujita for their technical assistance. This work was supported by a Grant-in-Aid for Scientific Research, Developmental Scientific Research, and Scientific Research on Priority Areas from the Ministry of Education, Science, Sports, and Culture and by the Program for Promotion of Fundamental Studies in Health Sciences of the Organization for Drug ADR Relief, R&D Promotion and Product Review of Japan (to I.K.) and Japan Research Foundation for Clinical Pharmacology (to T.M.).

COMPETING INTERESTS STATEMENTS

The authors declare that they have no competing financial interests.

Received 8 September 2004; accepted 19 January 2005
Published online at http://www.nature.com/naturemedicine/

1. Orlic, D. *et al.* Mobilized bone marrow cells repair the infarcted heart, improving function and survival. *Proc. Natl. Acad. Sci. USA* **98**, 10344–10349 (2001).
2. Ohtsuka, M. *et al.* Cytokine therapy prevents left ventricular remodeling and dysfunction after myocardial infarction through neovascularization. *FASEB J.* **18**, 851–853 (2004).
3. Moon, C. *et al.* Erythropoietin reduces myocardial infarction and left ventricular functional decline after coronary artery ligation in rats. *Proc. Natl. Acad. Sci. USA* **100**, 11612–11617 (2003).
4. Parsa, C.J. *et al.* A novel protective effect of erythropoietin in the infarcted heart. *J. Clin. Invest.* **112**, 999–1007 (2003).
5. Zou, Y. *et al.* Leukemia inhibitory factor enhances survival of cardiomyocytes and induces regeneration of myocardium after myocardial infarction. *Circulation* **108**, 748–753 (2003).
6. Minatoguchi, S. *et al.* Acceleration of the healing process and myocardial regeneration may be important as a mechanism of improvement of cardiac function and remodeling by postinfarction granulocyte colony-stimulating factor treatment. *Circulation* **109**, 2572–2580 (2004).
7. Adachi, Y. *et al.* G-CSF treatment increases side population cell infiltration after myocardial infarction in mice. *J. Mol. Cell. Cardiol.* **36**, 707–710 (2004).
8. Kawada, H. *et al.* Nonhematopoietic mesenchymal stem cells can be mobilized and differentiate into cardiomyocytes after myocardial infarction. *Blood* **104**, 3581–3587 (2004).
9. Avalos, B.R. Molecular analysis of the granulocyte colony-stimulating factor receptor. *Blood* **88**, 761–777 (1996).
10. Demetri, G.D. & Griffin, J.D. Granulocyte colony-stimulating factor and its receptor. *Blood* **78**, 2791–808 (1991).
11. Berliner, N. *et al.* Granulocyte colony-stimulating factor induction of normal human bone marrow progenitors results in neutrophil-specific gene expression. *Blood* **85**, 799–803 (1995).
12. Orlic, D. *et al.* Bone marrow cells regenerate infarcted myocardium. *Nature* **410**, 701–705 (2001).
13. Asahara, T. *et al.* Bone marrow origin of endothelial progenitor cells responsible for postnatal vasculogenesis in physiological and pathological neovascularization. *Circ. Res.* **85**, 221–228 (1999).
14. Kocher, A.A. *et al.* Neovascularization of ischemic myocardium by human bone-marrow-derived angioblasts prevents cardiomyocyte apoptosis, reduces remodeling and improves cardiac function. *Nat. Med.* **7**, 430–436 (2001).
15. Jackson, K.A. *et al.* Regeneration of ischemic cardiac muscle and vascular endothelium by adult stem cells. *J. Clin. Invest.* **107**, 1395–1402 (2001).
16. Balsam, L.B. *et al.* Haematopoietic stem cells adopt mature haematopoietic fates in ischaemic myocardium. *Nature* **428**, 668–673 (2004).
17. Murry, C.E. *et al.* Haematopoietic stem cells do not transdifferentiate into cardiac myocytes in myocardial infarcts. *Nature* **428**, 664–668 (2004).
18. Norol, F. *et al.* Influence of mobilized stem cells on myocardial infarct repair in a nonhuman primate model. *Blood* **102**, 4361–4368 (2003).
19. Aarts, L.H., Roovers, O., Ward, A.C. & Touw, I.P. Receptor activation and 2 distinct COOH-terminal motifs control G-CSF receptor distribution and internalization kinetics. *Blood* **103**, 571–579 (2004).
20. Benekli, M., Baer, M.R., Baumann, H. & Wetzler, M. Signal transducer and activator of transcription proteins in leukemias. *Blood* **101**, 2940–2954 (2003).
21. Smithgall, T.E. *et al.* Control of myeloid differentiation and survival by Stats. *Oncogene* **19**, 2612–2618 (2000).
22. Dumont, E.A. *et al.* Cardiomyocyte death induced by myocardial ischemia and reperfusion: measurement with recombinant human annexin-V in a mouse model. *Circulation* **102**, 1564–1568 (2000).
23. van Heerde, W.L. *et al.* Markers of apoptosis in cardiovascular tissues: focus on Annexin V. *Cardiovasc. Res.* **45**, 549–559 (2000).
24. Bromberg, J. Stat proteins and oncogenesis. *J. Clin. Invest.* **109**, 1139–1142 (2002).
25. El-Adawi, H. *et al.* The functional role of the JAK-STAT pathway in post-infarction remodeling. *Cardiovasc. Res.* **57**, 129–138 (2003).
26. Matsuura, K. *et al.* Adult cardiac Sca-1-positive cells differentiate into beating cardiomyocytes. *J. Biol. Chem.* **279**, 11384–11391 (2004).
27. Zou, Y. *et al.* Both Gs and Gi proteins are critically involved in isoproterenol-induced cardiomyocyte hypertrophy. *J. Biol. Chem.* **274**, 9760–9770 (1999).
28. Funamoto, M. *et al.* Signal transducer and activator of transcription 3 is required for glycoprotein 130-mediated induction of vascular endothelial growth factor in cardiac myocytes. *J. Biol. Chem.* **275**, 10561–10566 (2000).
29. Ikeda, K. *et al.* The effects of sarpogrelate on cardiomyocyte hypertrophy. *Life Sci.* **67**, 2991–2996 (2000).

Cell Tissue Res (2004) 316:141–153
DOI 10.1007/s00441-004-0862-1

REGULAR ARTICLE

Kohei Tsuchiya · Taisuke Mori · Guoping Chen · Takashi Ushida · Tetsuya Tateishi · Takeo Matsuno · Michiie Sakamoto · Akihiro Umezawa

Custom-shaping system for bone regeneration by seeding marrow stromal cells onto a web-like biodegradable hybrid sheet

Received: 28 August 2003 / Accepted: 23 January 2004 / Published online: 4 March 2004

Abstract New bone for the repair or the restoration of the function of traumatized, damaged, or lost bone is a major clinical need, and bone tissue engineering has been heralded as an alternative strategy for regenerating bone. A novel web-like structured biodegradable hybrid sheet has been developed for bone tissue engineering by preparing knitted poly(DL-lactic-*co*-glycolic acid) sheets (PLGA sheets) with collagen microsponges in their openings. The PLGA skeleton facilitates the formation of the hybrid sheets into desired shapes, and the collagen microsponges in the pores of the PLGA sheet promote cell adhesion and uniform cell distribution throughout the sheet. A large number of osteoblasts established from marrow stroma adhere to the scaffolds and generate the desired-shaped bone in combination with these novel sheets. These results indicate that the web-like structured novel sheet shows promise for use as a tool for custom-shaped bone regeneration in basic research on osteogenesis and for the development of therapeutic applications.

Keywords Bone regeneration · Tissue engineering · Scaffold · Marrow stroma · Polymer · KUSA-A1 cells

This work was supported in part by a grant from the Ministry of Education, Culture, Sports, Science, and Technology of Japan, Health and Labour Sciences Research Grants (translational research), and the Organization for Pharmaceutical Safety and Research (to A.U.)

K. Tsuchiya · T. Mori · A. Umezawa (✉)
Department of Reproductive Biology and Pathology,
National Research Institute for Child and Health Development,
Okura, Setagaya, 157-8535 Tokyo, Japan
e-mail: umezawa@1985.jukuin.keio.ac.jp

K. Tsuchiya · T. Mori · M. Sakamoto
Department of Pathology,
Keio University School of Medicine,
160-8582 Tokyo, Japan

K. Tsuchiya · T. Matsuno
Department of Orthopedic Surgery,
Asahikawa Medical College,
078-8802 Hokkaido, Japan

K. Tsuchiya · G. Chen · T. Tateishi
Biomaterials Center,
National Institute for Materials Science,
305-0044 Ibaraki, Japan

G. Chen · T. Ushida
Tissue Engineering Research Center,
National Institute of Advanced Industrial Science and Technology,
661-0974 Hyogo, Japan

T. Ushida
Center for Disease Biology and Integrative Medicine,
School of Medicine, University of Tokyo,
113-0033 Tokyo, Japan

Introduction

New bone for the replacement or restoration of the function of traumatized, damaged, or lost bone is a major clinical and socioeconomic need. Bone formation strategies, although attractive, have yet to yield functional and mechanically competent bone. Autografts (bone obtained from another site in the same subject of the same species) are currently the gold standard for bone repair and substitution, but the use of autografts has several serious disadvantages, such as additional expense and trauma to the patient, the possibility of donor-site morbidity, and limited availability (Glowacki and Mulliken 1985; Bauer and Muschler 2000). Because of these problems, bone tissue engineering has been heralded as an alternative strategy for the regeneration of bone (Langer and Vacanti 1993; Crane et al. 1995; Boyan et al. 1999).

Bone has a highly organized structure composed of a calcified connective tissue matrix formed by the proliferation and differentiation of osteoprogenitors into mature osteoblasts (Maniatopoulos et al. 1988; Pitaru et al. 1993). The osteoblasts belong to the stromal fibroblastic system of the bone marrow, which contains other stromal cells, such as chondrocytes and myoblasts (Friedenstein 1976; Owen and Friedenstein 1988; Haynesworth et al. 1992). We have shown that mouse stromal cells are able to differentiate into cardiomyocytes (Makino et al. 1999;

Gojo et al. 2003), endothelial cells, neuronal cells (Kohyama et al. 2001), and adipocytes (Umezawa et al. 1991). We have previously established a murine osteoblast cell line, KUSA-A1, and shown that clonal stromal cells can generate bone in vivo (Umezawa et al. 1992). Marrow stromal cells are expected to serve as a good source for cell therapy, in addition to embryonic stem cells and fetal cells. Although these precursor cells have been reported to be stem cells, it remains unknown as to whether they are homogeneous or whether they constitute subpopulations of cells committed to various lineages of differentiation (Owen and Friedenstein 1988). The acquisition of a large number of osteoblast precursors as a cell source and the control of differentiation are essential to the success of the production of tissue-engineered bone for clinical application (Minuth et al. 1998).

Temporary three-dimensional scaffolds play an important role in the manipulation of the functions of osteoblasts (Chicurel et al. 1998) and in the guidance of the formation of new bones into the desired shapes (Ishaug et al. 1997; Ishaug-Riley et al. 1998), in the bone tissue-engineering approach. These scaffolds should be biocompatible, osteoconductive, biodegradable, highly porous with a large surface-to-volume ratio, mechanically strong, and malleable into the desired shapes. Synthetic polymers, such as poly(lactic acid), poly(glycolic acid), and poly(DL-lactic-*co*-glycolic acid), which is abbreviated here as PLGA, are easily processed into the desired shapes and are mechanically strong (Langer and Vacanti 1993; Ishaug et al. 1997; Ishaug-Riley et al. 1998; Mikos et al. 1998). Moreover, their degradation time can be manipulated by controlling their crystallinity, molecular weight, and the ratio of lactic acid to glycolic acid copolymer (Thomson et al. 1995). Collagen is the primary component of extracellular bone matrix and has been demonstrated to produce good osteoconductivity (Aronow et al. 1990). Synthetic polymers, on the other hand, lack cell recognition signals, and their hydrophobic properties hinder the uniform seeding of cells in three dimensions. However, since collagen scaffolds are mechanically weak, these materials have been hybridized to combine their advantages and provide excellent three-dimensional porous biomaterials for bone tissue engineering.

We have developed collagen-hybridized PLGA sponge and have reported good biocompatibility both for cartilage tissue engineering with mature bovine chondrocytes (Sato et al. 2001; Chen et al. 2003) and for bone tissue engineering with osteoblasts isolated from marrow cells (Ochi et al. 2003). The sponges organize satisfactory cartilage and bone tissue when the cells fill the pores of the scaffold. The uniform distribution of the cells throughout the scaffolds is imperative for the development of homogeneous tissue, but special seeding techniques, such as stir flask culture or perfusion bioreactor culture, are required to produce an even distribution reliably (Vunjak-Novakovic et al. 1998; Freed et al. 1999). Since simple static seeding methods tend to produce an uneven distribution with large patches of cells on the surface, we have hybridized collagen microsponges with PLGA sheets. The sheets have a collagen fiber network in the openings of the PLGA fiber sheets. The findings that the sheets trap cells, that they can be laminated or rolled to control their shape for tissue engineering, and that they also have the capacity to supply minerals by depositing apatite particulates on the surface of collagen microsponges indicate their great advantages. In this study, we have shown that, when the novel web-like structured sheets are used as a scaffold for bone tissue engineering, an even cell distribution and the control of its shape can be achieved.

Materials and methods

Scaffold fabrication

The hybrid sheet was prepared by allowing collagen microsponges to form in the openings of PLGA knitted sheets as previously described (Chen et al. 2003). Briefly, as shown in Fig. 1A, a knitted Vicryl sheet made of polylactin 910 (a 90:10 co-polymer of glycolic acid and lactic acid) was immersed in a type I bovine collagen acidic solution (pH 3.2, 0.5% by weight, Koken, Tokyo, Japan) and frozen at −80°C for 12 h. It was then freeze-dried under vacuum (0.2 Torr) for 24 h to allow the formation of collagen microsponges. The collagen microsponges were further cross-linked by treatment with glutaraldehyde vapor saturated with a 25% aqueous glutaraldehyde solution at 37°C for 4 h. After the cross-linking, the sponge was treated with a 0.1 M aqueous glycine solution to block unreacted aldehyde groups. After being washed with deionized water and freeze-dried, the collagen-hybridized PLGA (PLGA/COL) sheet was complete. The sheets were sterilized with ethylene oxide for cell culture.

Cell culture

KUSA-A1 cells were cultured as described previously (Umezawa et al. 1992; Kohyama et al. 2001; Ochi et al. 2003).

Cell seeding of a PLGA/COL sheet

A PLGA/COL sheet was placed into a 100-mm culture dish (Falcon) and covered with a silicone rubber framework. A 2-ml volume of KUSA-A1 cell suspension at a density of 5×10^6/ml was dropped onto the PLGA/COL sheet (area: 4 cm^2). After cultivation for 6 h, the sheet was turned over and re-seeded with the same number of cells on the reverse side. For comparison, a KUSA-A1 suspension (1×10^7 cells/ml) was injected into collagen hybrid PLGA sponges, and the injected sponges were incubated at 37°C for more than 30 min. The sponges were then transplanted into the subcutaneous tissue of C3H mice as previously described (Ochi et al. 2003).

Scanning electron microscopy

PLGA sheets and PLGA/COL sheets were examined by scanning electron microscopy (SEM). They were cut into small pieces with scissors and coated with gold by means of a sputter coater (Sanyu Denshi, Tokyo, Japan; gas pressure: 50 mtorr, current: 5 mA, coating time: 180 s). The samples were examined with a JSM-6400Fs scanning electron microscope (JEOL, Tokyo, Japan) operated at a voltage of 3 kV.

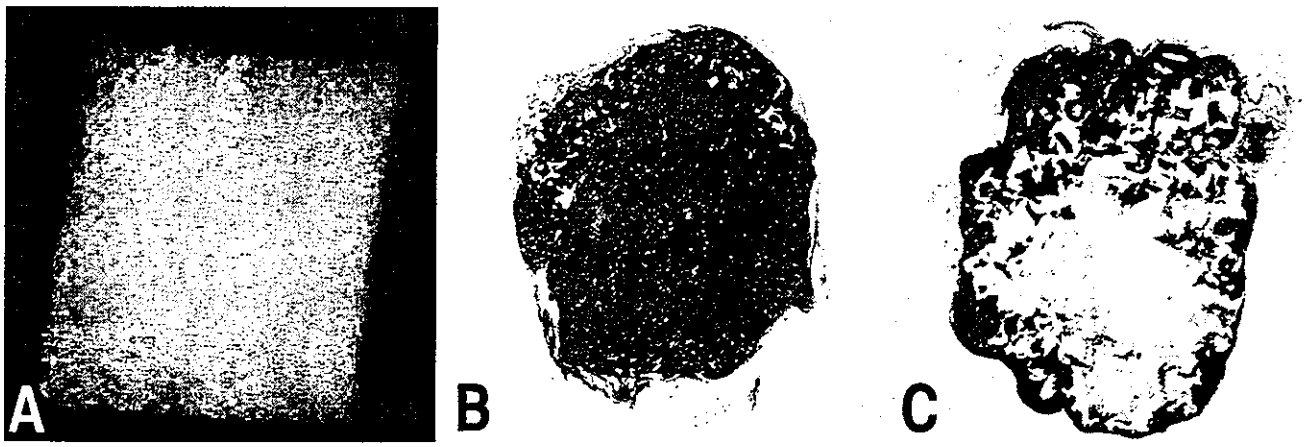

Fig. 1A–C Bone formation in collagen hybrid PLGA sponge. Macroscopic appearance of the collagen hybrid PLGA sponge (A). Complete bone formation of an in vivo 4-week construct based on KUSA-A1 cells and collagen hybrid PLGA sponge (B). Some constructs showed uneven bone distribution. Living cells did not completely fill the pore cavities of the sponge (C). ×5

Transmission electron microscopy

Samples cultured in vitro for 1 day and 2 weeks were examined by transmission electron microscopy (TEM). They were fixed in 2.5% glutaraldehyde, postfixed in 1% osmium tetroxide, dehydrated, and embedded in resin. Ultrathin sections (70–90 nm) were cut and stained with 2% uranyl acetate and Reynold's lead citrate before being examined with a JEM-1200 EX microscope (JOEL) at 80 kV.

In vivo assay

All animals received humane care in compliance with the "Principles of Laboratory Animal Care" formulated by the National Society for Medical Research and the "Guide for the Care and Use of Laboratory Animals" prepared by the Institute of Laboratory Animal Resources and published by the US National Institutes of Health (NIH Publication no. 86–23, revised 1985). The operation protocols were accepted by the Laboratory Animal Care and Use Committee of the National Research Institute for Child and Health Development (Tokyo) and by Keio University School of Medicine.

Laminated sheet implantation onto calvarial defects

Surgery was performed under anesthesia with Nembutal (50 mg/kg, i.p.). A midline skin incision approximately 1 cm long was made on the dorsal surface of the cranium, and the periosteum was removed. A 4.3-mm-diameter full-thickness circular defect was created in the skull with a trephine bar (Hasegawa Medical, Tokyo, Japan) attached to an electric handpiece, with minimal penetration of the dura. The defect was covered with three sheets of cell-loaded scaffolds cut to fit the shape of the defect. The scalp was then closed with 6-0 nylon sutures, and the animals were given access to food and allowed to behave *ad libitum*. Ten defects were left untreated, 10 defects were treated with PLGA/COL sheets alone as controls, and 10 defects were filled with PLGA/COL sheets seeded with KUSA-A1 cells.

Custom-shaped bone formation in mice

With the aim of producing long bone, cylinder-like bone was formed by rolling KUSA-A1-seeded sheets around a silicone rod 3 mm in diameter. The ends of the sheets were hemmed with 4-0 Vicryl dissolvable stitches. The rolled sheets were transplanted into subcutaneous tissue for 4 weeks, flat or after being knotted. Tissue-engineered phalanges were formed in a similar manner. KUSA-A1-seeded sheets were wrapped around a silicone rubber block trimmed in advance to the shape of the distal phalanx and transplanted into subcutaneous tissue. After cultivation in syngeneic C3H/He mice, NOD/SCID mice, and NOD/SCID/IL2-receptor γ knock-out immunodeficient mice (NOG), the specimens were extracted and examined histologically.

Histological and Immunohistochemical staining

Calvaria, femurs, and subcutaneous specimens were dissected at various times after implantation and fixed and decalcified for 1 week in 10% EDTA (pH 8.0) solution. After dehydration in ascending concentrations of ethanol and xylene, the transplants were embedded in paraffin and sectioned. The paraffin sections were then deparaffinized, hydrated, and either were stained with hematoxylin and eosin or were immunohistochemically stained with anti-human Factor VIII mAb (DAKO, Carpenteria, Calif.) to detect angiogenesis.

Results

Bone distribution of sponges

We previously reported that KUSA-A1 cells generated cuboidal bone when used in combination with PLGA/COL hybrid sponge. In those experiments, the KUSA-A1 cells were distributed evenly into sponges and had generated cuboidal bone in the subcutaneous tissue at 8 weeks (Fig. 1A, B); however, some of them exhibited uneven bone formation. The bone was generated mainly at the periphery of the sponge, like an eggshell (Fig. 1C).

Collagen-hybridized PLGA sheet

We developed the sheet-style scaffold to prevent uneven bone formation (Fig. 2A–C). The synthetic biodegradable polymer, PLGA, which was 200 μm thick, was hybridized with collagen microsponges. SEM analysis revealed that the collagen microsponges overlaid the interstices of the

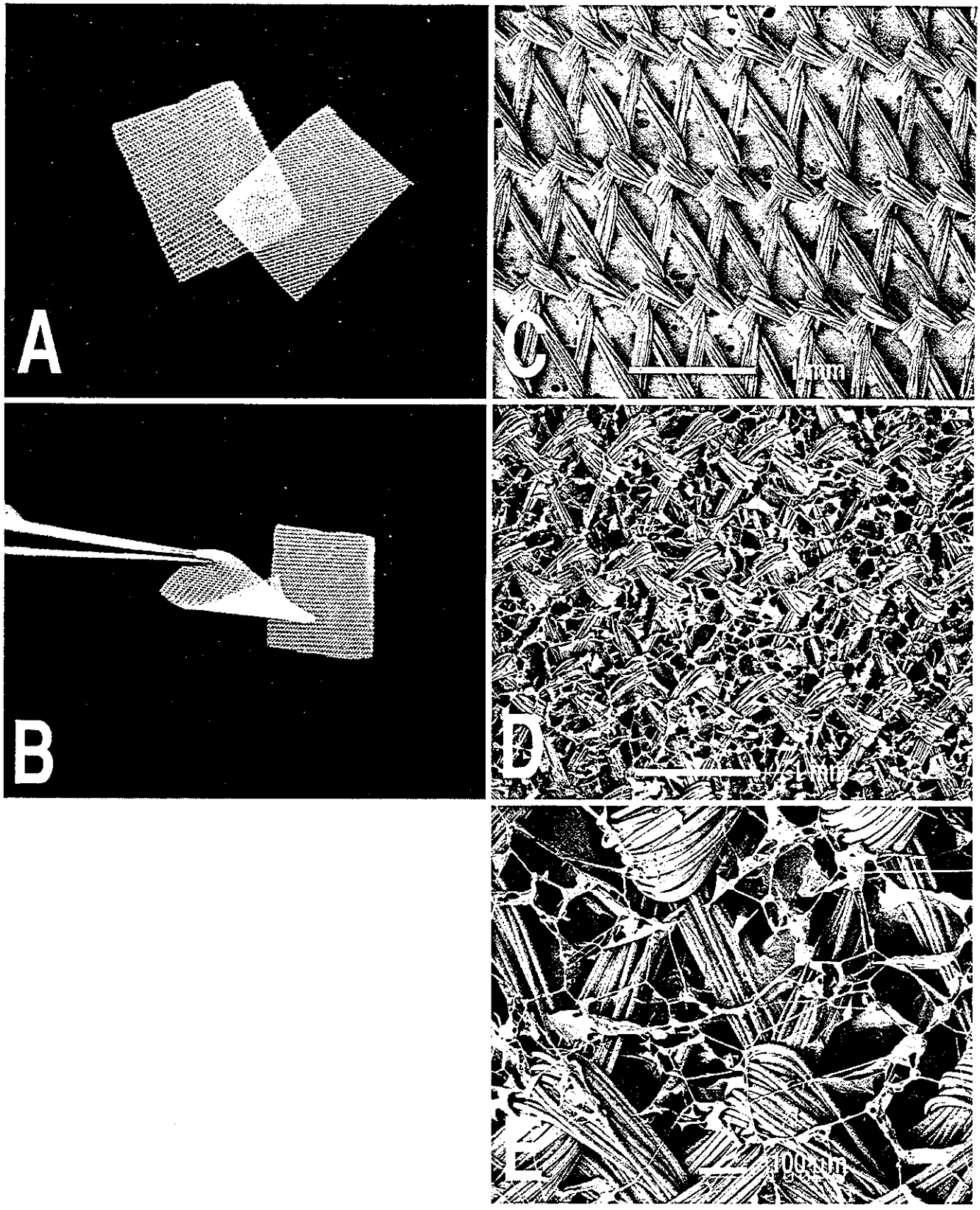

Fig. 2A–E Collagen hybrid PLGA sheet. The thin 200 µm sheets are easy to handle (**A, B**). SEM micrographs of a PLGA sheet without collagen (**C**) and a hybrid sheet with collagen (**D**). Higher magnification of the hybrid sheet (**E**)

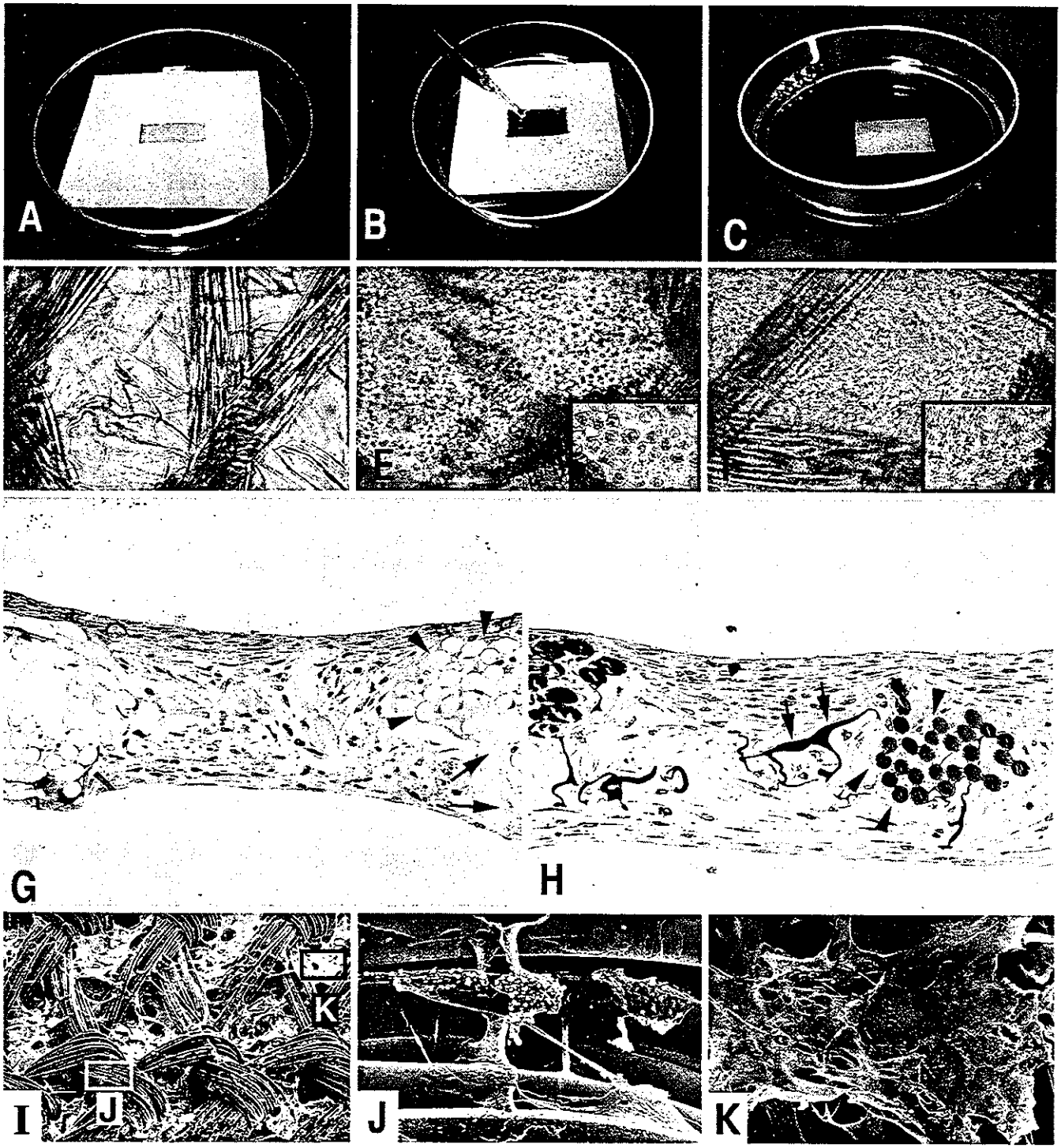

Fig. 3A–K Process of cell seeding. **A–C** Cell seeding of the sheet. The sheet was framed in silicone rubber (**A**), and the cell suspension was simply dropped onto the sheet (**B**). The silicone rubber was removed 6 h after seeding, and the sheet was cultured in growth medium (**C**). **D–F** Phase-contrast micrographs of a cell-seeded sheet. The openings of the PLGA/COL sheet (**D**) were filled with cells at 30 min (**E**) and were completely covered with abundant extracellular matrix at 1 week (**F**). **G, H** Toluidine-blue stained cross sections of the cell-seeded sheet at 1 day (**G**) and 2 weeks (**H**). The thickness of the sheet had increased (*arrowheads* PLGA fibers, *arrows* collagen fibers). **I–K** SEM micrographs of a PLGA/COL sheet after cell seeding. A portion of PLGA fiber (**J**) and collagen microsponge (**K**) are shown. **D–F** ×200, **G, H** ×400, **I** ×50, **J, K** ×200

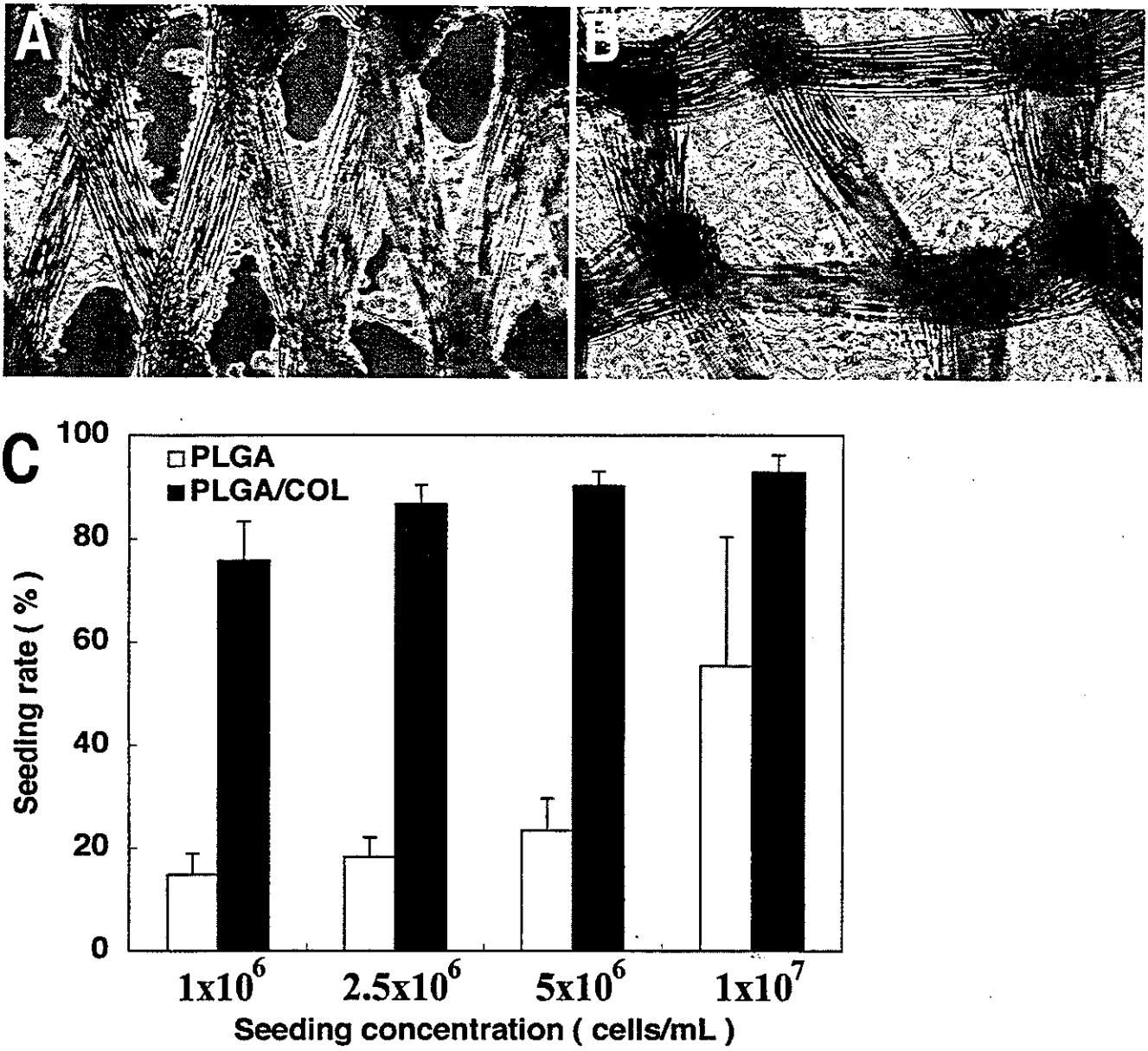

Fig. 4A–C Effect of collagen microsponges on cell adhesion. Microscopic appearance of a PLGA sheet (**A**) and PLGA/COL (**B**) sheet 1 day after seeding the same number of cells in suspension (1×10^7 cells). The seeding rates (**C**) indicate the differences in the number of adhering cells between the two sheets at the initial cell seeding concentrations. **A, B** ×100

fabricated web-like PLGA sheets (Fig. 2D, E). This structure was expected to entrap a large number of cells.

Cells uniformly trapped in sheets with a web-like pattern

A cell suspension was simply dropped onto the sheets (Fig. 3A–C), and the collagen microsponges had filled with precipitated cells 30 min after seeding. The cells had adhered completely at 3 h (Fig. 3D–F), whereas the non-hybridized PLGA sheets did not trap cells efficiently. The cells continued to spread and generate matrix over the sheets, so that at 2 weeks, the sheets were completely covered by extracellular matrix, and the thickness of sheet had increased (Fig. 3G, H). After in vitro culture for 1 day, SEM examination revealed the preference of cells for components of the scaffold (Fig. 3I–K). A large number of cells had adhered to the collagen microsponge portion rather than to the PLGA fibers. Since synthetic polymers lack cell recognition signals, and since their hydrophobic properties hinder cell adhesion, the hybridization of collagen microsponges was advantageous in achieving cell retention.

The PLGA/COL sheets trapped significantly more cells than non-hybridized control PLGA sheets (Fig. 4A, B). The numbers of cells that had adhered to the sheets at 6 h after seeding increased with the initial cell seeding concentration (Fig. 4C).